Article

Neuron

Tau Prion Strains Dictate Patterns of Cell Pathology, Progression Rate, and Regional Vulnerability In Vivo

Highlights

- Tau forms multiple, unique prion strains with distinct biochemical properties
- Tau strains induce diverse pathological phenotypes in vitro and in vivo
- Tau strains target different brain regions and propagate pathology at unique rates
- We present a framework to understand the diversity of human tauopathies

Authors

Sarah K. Kaufman, David W. Sanders, Talitha L. Thomas, ..., Apurwa M. Sharma, Timothy M. Miller, Marc I. Diamond

Correspondence

marc.diamond@utsouthwestern.edu

In Brief

Kaufman et al. observe that tau forms multiple self-propagating amyloid strains. The introduction of each into transgenic mouse brain creates a distinct pathology that targets different brain regions and induces unique rates of spread. Thus, strain variation can account for the diversity of human tauopathies.

Kaufman et al., 2016, Neuron *92*, 796–812
November 23, 2016
http://dx.doi.org/10.1016/j.neuron.2016.09.055

CellPress

Tau Prion Strains Dictate Patterns of Cell Pathology, Progression Rate, and Regional Vulnerability In Vivo

Sarah K. Kaufman,[1,3,5] David W. Sanders,[1,3,5] Talitha L. Thomas,[3] Allison J. Ruchinskas,[3] Jaime Vaquer-Alicea,[3] Apurwa M. Sharma,[3,4] Timothy M. Miller,[2] and Marc I. Diamond[3,6,*]
[1]Program in Neuroscience
[2]Department of Neurology
Washington University in St. Louis, St. Louis, MO 63130, USA
[3]Center for Alzheimer's and Neurodegenerative Diseases, University of Texas Southwestern Medical Center, Dallas, TX 75390, USA0, USA
[4]Program in Biochemistry, Washington University in St. Louis, St. Louis, MO 63130, USA
[5]Co-first author
[6]Lead Contact
*Correspondence: marc.diamond@utsouthwestern.edu
http://dx.doi.org/10.1016/j.neuron.2016.09.055

SUMMARY

Tauopathies are neurodegenerative disorders that affect distinct brain regions, progress at different rates, and exhibit specific patterns of tau accumulation. The source of this diversity is unknown. We previously characterized two tau strains that stably maintain unique conformations in vitro and in vivo, but did not determine the relationship of each strain to parameters that discriminate between tauopathies such as regional vulnerability or rate of spread. We have now isolated and characterized 18 tau strains in cells based on detailed biochemical and biological criteria. Inoculation of PS19 transgenic tau (P301S) mice with these strains causes strain-specific intracellular pathology in distinct cell types and brain regions, and induces different rates of network propagation. In this system, strains alone are sufficient to account for diverse neuropathological presentations, similar to those that define human tauopathies. Further study of these strains can thus establish a structural logic that governs these biological effects.

INTRODUCTION

Tauopathies are a diverse group of neurodegenerative diseases characterized by clinical heterogeneity, progressive deposition of tau protein aggregates in characteristic brain regions, and distinct cellular pathologies (Lee et al., 2001). The etiology of this clinical and pathological diversity is unknown, but may hold the key to accurate diagnosis, prognosis, and therapy. Tauopathies include Alzheimer's disease (AD), frontotemporal dementias (FTDs), corticobasal degeneration (CBD), progressive supranuclear palsy (PSP), and others (Lee et al., 2001). Most tauopathies are sporadic, but dominantly inherited mutations in the *MAPT* gene, which encodes the tau protein, lead to specific FTD syndromes (Hutton et al., 1998). Disease-associated mutations enhance the ability of tau to form amyloids, which are ordered protein assemblies rich in cross beta sheet structure (Knowles et al., 2014), and support a causal role for tau aggregation in pathogenesis (Barghorn et al., 2000).

In AD, the most common tauopathy (Lee et al., 2001), tau amyloid deposition occurs in an orderly fashion, beginning in the transentorhinal cortex, spreading to synaptically connected regions such as the hippocampus, and eventually moving to more distant regions of the neocortex (Braak and Braak, 1991). Multiple studies have now documented tau aggregate uptake, "seeding" (i.e., aggregate serving as a template for the conversion of monomer to a fibrillar form) and transfer of aggregates among cultured cells (Frost et al., 2009a; Guo and Lee, 2011; Holmes et al., 2013; Nonaka et al., 2010). Experimental evidence suggests that "propagation", or the movement of tau aggregates between connected neurons with seeding of tau monomer in recipient cells, mediates this progression in vivo (Sanders et al., 2016; Walker and Jucker, 2015). Importantly, injection of tau aggregates into mice that express human tau protein induces tau pathology that spreads outward along known brain networks (Clavaguera et al., 2009; Iba et al., 2013). Transgenic mice that limit the expression of tau to the entorhinal cortex also show spread of tau pathology to distant, connected brain regions (de Calignon et al., 2012; Liu et al., 2012). Together, these studies suggest that propagation of an aggregated state underlies the progression of tau pathology. These observations match the established mechanisms of propagation of pathological prion protein (PrP) (Prusiner, 1998).

The pathology of tauopathies occurs in distinct brain regions (Arnold et al., 2013), involves disparate brain networks (Raj et al., 2012; Zhou et al., 2012), and features unique tau inclusions in various cell types (Kovacs, 2015). Individuals may develop rapid or slow neurodegeneration even within the same syndrome (Armstrong et al., 2014; Thalhauser and Komarova, 2012). The basis of these diverse disease patterns is unknown.

We initially observed that tau adopts multiple, stably propagating conformers in vitro and speculated that structural variation in amyloids could underlie different tauopathies (Frost

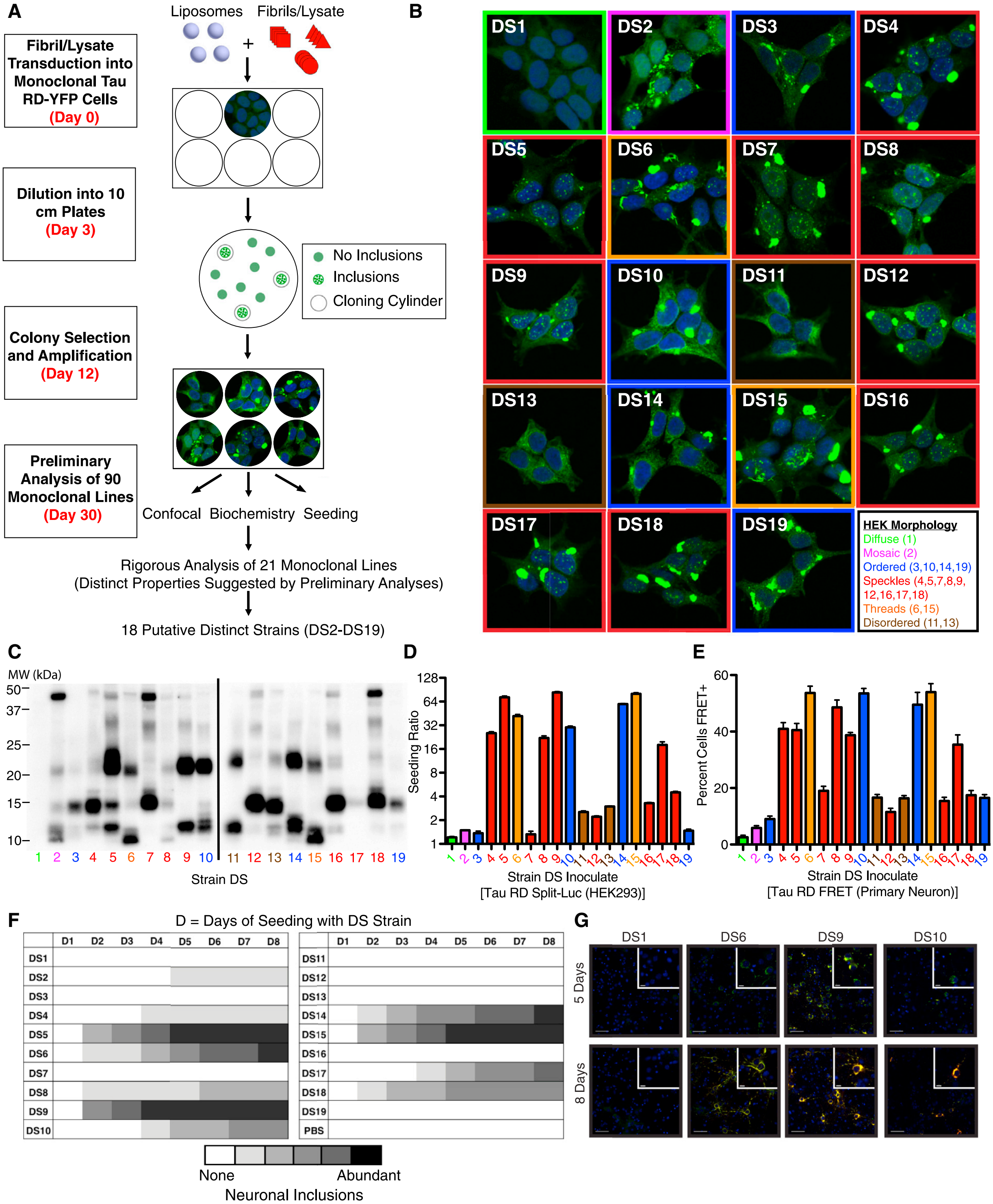

Figure 1. Generation and Characterization of a Tau Prion Strain Library

(A) A monoclonal HEK293 line stably expressing tau RD(P301L/V337M) ("LM")-YFP (DS1) was treated with diverse sources of fibrillar tau seeds. 90 monoclonal lines that stably propagated tau inclusions were derived and characterized by the indicated metrics. 18 strains were differentiated based on their unique properties in the indicated assays. See Figure S1A for origin of inoculates used to derive each strain.

(B) Several tau inclusion phenotypes were identified in the monoclonal strains: mosaic (magenta), ordered (blue), speckles (red), threads (orange), and disordered (brown). With the exception of the mosaic phenotype, these inclusion phenotypes stably propagate to daughter cells over months of division. A negative control cell line (DS1) features diffuse tau (green). See Figures S2F–S2H for data regarding stability of specific strains upon passage into DS1.

(legend continued on next page)

et al., 2009b). We subsequently determined that tau forms discrete prion "strains" that propagate with remarkable fidelity through living systems (Sanders et al., 2014). The concept of prion strains derived from a realization that PrP prions can induce distinct transmissible spongiform encephalopathies with reproducible incubation times and patterns of neuropathology (Collinge and Clarke, 2007). It is now clear that PrP prion strains derive from different PrP amyloid conformations and produce predictable incubation times and neurodegenerative phenotypes upon serial passage in vivo. Moreover, distinct PrP strains probably account for the myriad features of individual PrP prion diseases (Collinge et al., 1996). The concept of a strain as a stably propagating structure that induces a specific and reproducible phenotype is critical, as it anticipates and enables mechanistic, diagnostic, and therapeutic insights based on knowledge of a defined molecular assembly (Sanders et al., 2016).

In addition to the distinct morphologies of tau fibrils and isoform composition of amyloid deposits in tauopathies (Lee et al., 2001), prior studies have suggested that unique tau amyloid structures might account for some aspects of clinical variation. Injection of homogenate from different tauopathy brains into a mouse model that expresses full-length human tau induced pathology that closely resembled that of the human source cases (Clavaguera et al., 2013). In a similar study, tau aggregates purified either from AD or CBD brains induced distinct patterns of tau pathology that affected different cell populations in transgenic mice that express 1N4R tau with a P301S mutation (PS19) (Boluda et al., 2015). However, both works relied upon a limited number of patient samples that likely contain a heterogeneous mixture of tau aggregate conformations (Sanders et al., 2014). Thus, the structure and biochemical properties of injected tau aggregates could not be well defined, making it impossible to directly link an amyloid structure to pathology.

Like PrP, tau forms bona fide prion strains that propagate in cells and animals (Sanders et al., 2014). We have now isolated 18 putative tau prion strains derived from recombinant, mouse, or human sources. We have studied them extensively in vivo and find that they can account for diverse and predictable patterns of neuropathology. This work thus develops a framework to understand the relationship of tau prion structure to distinct tauopathy syndromes.

RESULTS

Generation of a Library of Tau Strains

We previously created a monoclonal HEK293 cell line (Clone 1/DS1) that stably expresses the repeat domain (amino acids 244–372) of 2N4R tau with two disease-associated mutations (P301L and V337M), which allows us to indefinitely propagate tau prion strains derived from a variety of sources (Sanders et al., 2014). We treated DS1 cells with tau aggregates from diverse recombinant, mouse, and human brain samples (Figure 1A). We isolated and amplified 90 monoclonal cell lines that stably propagated tau aggregates and froze them for later study. Following preliminary analyses by several assays (inclusion morphology, limited proteolysis, and seeding by tau split-luciferase complementation, as described previously; Sanders et al., 2014), we isolated 18 putatively distinct strains (DS2–DS19; see Figure S1A for origin of each strain). These strains featured several striking differences in their subcellular distribution of aggregated tau (Figure 1B): a single, large juxtanuclear inclusion (ordered: DS3, DS10, DS14, and DS19), prominent nuclear inclusions (speckles: DS4, DS5, DS7, DS8, DS9, DS12, DS16, DS17, and DS18), aggregated tau that failed to organize into ordered inclusions (disordered: DS11 and DS13), fibril-like ribbons of aggregated tau throughout the cytoplasm (threads: DS6 and DS15), and one strain that sectored with time, reverting from the aggregated state to the soluble diffuse state (mosaic: DS2). Importantly, with the exception of the mosaic strain DS2, every daughter cell featured the same inclusion morphology even after months of passage, suggesting that each monoclonal cell line stably propagated a single strain.

To examine whether the tau inclusions were composed of structurally distinct tau amyloids, we used limited proteolysis, an assay previously shown to differentiate prion strains derived from PrP (Bessen and Marsh, 1994) and tau (Sanders et al., 2014). We thus determined a "fingerprint" for each putative strain based on the regions of tau protected from digestion by pronase (Figure 1C). These digestion patterns were stable even upon dilution with HEK lysate (Figure S1B), confirming their independence from the amount of aggregated tau present in each sample. This assay suggested that while cell lines with different inclusion morphologies always propagated different

(C) Limited proteolysis using pronase differentiates the protected fibrillar cores in individual tau strains. Unique fingerprints along with other metrics indicated structurally distinct tau prion strains. See Figure S1B for pronase digestion of strains diluted with HEK lysate.

(D) Seeding activity of strains in a split-luciferase assay. A tau RD(P301S) split-luciferase assay based on enzymatic complementation following aggregation demonstrates differences in strain seeding activities following introduction into the cytoplasm using lipofectamine. The seeding ratio indicates luminescence relative to sham treatment. The biological quadruplicates with saturating quantities of lysate were averaged. The error bars represent SEM for biological quadruplicates.

(E) Strain seeding activities replicate in primary neurons expressing tau RD. Primary hippocampal neurons expressing tau RD(P301S)-CFP and tau RD(P301S)-YFP were treated with lysates derived from various strains. After 96 hr, neurons were fixed and the percentage of cells featuring seeded aggregates was determined by FRET flow cytometry. The error bars represent SEM for biological quintuplicates.

(F) Strain seeding activities replicate in primary neurons expressing full-length tau. Primary hippocampal neurons expressing 1N4R tau(P301S)-YFP were exposed to lysates from each strain and the extent of seeding was semiquantitatively determined at various time points (D = number of days) based on the extent of visible YFP puncta (0–5: 0 = none and 5 = abundant inclusions). The strains show variable lag times and extent of seeding, which correlates with the split-luciferase complementation assay.

(G) Strains differentially induce the formation of insoluble tau aggregates in primary neurons. Triton X-100 was used to remove soluble tau, and the primary neurons were stained for conformationally altered tau (MC1) 5 or 8 days following seeding. The strains show significant differences in seeding of aggregation in neurons. This parallels differences in the split-luciferase complementation assay. The scale bars represent 50 μm for the wide view and 10 μm for the inset images. See Figure S1C for representative images for all strains.

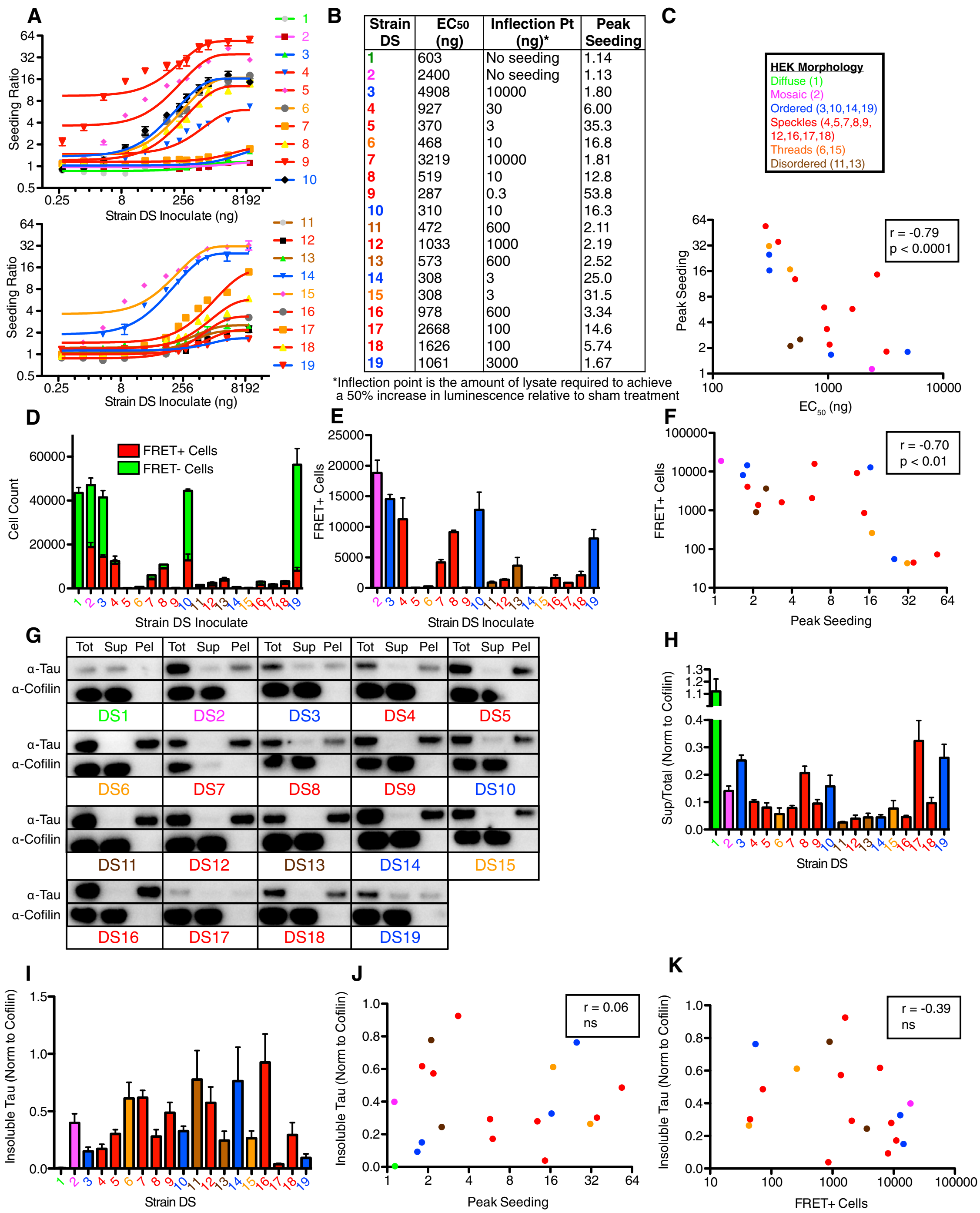

Strain DS	EC_{50} (ng)	Inflection Pt (ng)*	Peak Seeding
1	603	No seeding	1.14
2	2400	No seeding	1.13
3	4908	10000	1.80
4	927	30	6.00
5	370	3	35.3
6	468	10	16.8
7	3219	10000	1.81
8	519	10	12.8
9	287	0.3	53.8
10	310	10	16.3
11	472	600	2.11
12	1033	1000	2.19
13	573	600	2.52
14	308	3	25.0
15	308	3	31.5
16	978	600	3.34
17	2668	100	14.6
18	1626	100	5.74
19	1061	3000	1.67

*Inflection point is the amount of lysate required to achieve a 50% increase in luminescence relative to sham treatment

Figure 2. Seeding Activity, but Not Insoluble Tau, Correlates with Strain Toxicity In Vitro

(A) Strains have large differences in seeding of monomeric tau as determined by a tau split-luciferase complementation assay. The strain lysates were transduced into tau RD(P301S) split-luciferase cells, the seeding ratios relative to sham treatment were determined, and the titration curves were plotted using non-linear regression with a one-phase decay fit. The curves are plotted on two separate graphs for clarity. The error bars represent SEM for biological quadruplicates.

(B) Based on titration curves in the tau split-luciferase complementation assay, the EC_{50}, inflection point, and peak seeding ratio were determined for each strain. The inflection point represents the amount of lysate required to achieve a 50% increase in luminescence relative to sham treatment.

(C) Peak seeding significantly correlates with EC_{50}s for the strain library in the tau split-luciferase complementation assay.

(D) Strains display significant differences in toxicity. The strains were transduced in biological triplicates into cells overexpressing both tau RD(LM)-CFP and tau RD(LM)-YFP. After 72 hr, equivalent numbers of aggregate-containing (FRET+) cells were sorted for each condition by FRET flow cytometry. For the negative control (DS1), aggregate-negative (FRET−) cells were sorted. The sorted cells were allowed to proliferate in technical sextuplicates for 1 week.

(legend continued on next page)

conformations, inclusion morphology alone could not discriminate all strains.

Tau Strains Show Unique Seeding Profiles in Dividing Cells and Neurons

Next, we examined the ability of each putative strain to seed tau monomer using a cell line that expresses tau RD(P301S) fused to the N or C terminus of click beetle green luciferase enzyme (Mirbaha et al., 2015; Sanders et al., 2014). When saturating concentrations of lysate were transduced directly into the cytoplasm of these cells, induction of luminescence ranged from 0.3- to 80-fold increase in seeding at saturation versus background, termed the "seeding ratio" (Figure 1D). We observed no association between inclusion morphology and seeding. For example, the four ordered strains showed different seeding activity (DS3, DS10, DS14, and DS19). The relative seeding abilities of individual tau strains were largely recapitulated when lysates were applied to primary hippocampal neurons expressing tau RD(P301S) fluorescence resonance energy transfer (FRET) biosensor proteins (Holmes et al., 2014) (Figure 1E). We also observed these relative differences upon exposure of strains to primary neurons expressing full-length 1N4R P301S-YFP, suggesting common effects on either truncated or full-length tau. Strains also showed different lag phases to induce inclusions in neurons that express full-length tau (Figures 1F, 1G, and S1C).

Seeding Activity Correlates with Toxicity in Dividing Cells

To investigate the relationship between seeding activity and toxicity, we first performed a detailed titration of cell lysates (30 pg to 10 μg) from the 18 putatively distinct strains. We determined the EC_{50} and peak seeding ratio for each strain using the tau split-luciferase complementation assay. Strains differentially seeded tau monomer in cell culture as reflected by their peak seeding ratios (Figures 2A and 2B). Different strains displayed >10× range for EC_{50} (DS9: 287 ng and DS3: 4908 ng) (Figure 2B). Peak seeding and EC_{50} strongly anti-correlated (Figure 1C), suggesting that peak seeding accurately reflects a strain's potency in triggering tau aggregation.

We then compared the toxicity of each putative strain to their seeding potential. We generated a cell line (LM10) that expresses a mutant tau RD FRET pair (CFP/YFP) at high levels and assessed the growth potential of cells propagating various strains after first isolating aggregate-positive cells by FRET fluorescence-activated cell sorting (FACS) (Holmes et al., 2014). Several ordered and mosaic strains (DS2, DS3, DS10, and DS19) lost the aggregated state ("sectored") with repeated cell division (Figure 2D). All others stably propagated the aggregated state, but exhibited growth defects relative to LM10 cells that lacked tau aggregates (Figure 2E). Strains that sectored, a possible correlate of low seeding, were the least toxic. All three seeding metrics (peak seeding, EC_{50} and inflection point) correlated with inhibition of growth (Figures 2F, S2A, and S2B). In other words, strains that seeded more efficiently were significantly more toxic to cells that express high levels of monomeric tau.

We next performed sedimentation analyses to determine the level of soluble, insoluble, and total tau for all 18 putative strains (Figure 2G). While each strain (DS2–DS19) contained the majority of tau in the insoluble fraction (Figures 2G and 2H), different strains featured variable levels of insoluble (Figure 2I) and total (Figure S2C) tau. Neither total nor insoluble tau levels correlated with seeding (Figures 2J and S2D) or toxicity (Figures 2K and S2E). Thus, structural differences among strains, rather than soluble/insoluble tau levels per se, account for seeding activity and toxicity in dividing cells.

Diversity of Pathology Induced by Tau Strains

We hypothesized that to account for variation in tauopathies, individual tau strains should produce a wide array of pathological phenotypes in vivo. To test whether these putative strains can produce such diversity, we inoculated cell lysate from each line (DS1–DS19) into the PS19 mouse model that expresses 1N4R tau with the FTDP-17-associated P301S mutation from the prion promoter (Yoshiyama et al., 2007) (Figure 3A) and examined tau pathology induced 8 weeks after inoculation (Figures 3B–3J).

Pathology varied greatly between putative strains and was often, but not always, consistent with seeding activity observed in culture (Figures 1D–1G). Strains with low seeding activity (DS2, DS3, DS11, and DS19) produced a "rare seeding" phenotype in vivo, with limited AT8 pathology localized in CA1 of the ipsilateral hippocampus (Figures 3G and S3A). These strains appear

Aggregate-positive (FRET+) and aggregate-negative (FRET−) cells were then quantified by flow cytometry. The presence of FRET− cells in certain conditions reflects the fact that some strains lose the aggregated state with cell division. Technical sextuplicates were averaged for each biological replicate. The error bars represent SEM of biological triplicates.

(E) Aggregate-positive (FRET+) cells were quantified and plotted after 1 week of growth. This highlights the variable growth defects in aggregate-containing cells. The error bars represent SEM of biological triplicates.

(F) Toxicity correlates with seeding activity. The number of aggregate-positive (FRET+) cells for a strain was plotted against its peak seeding ratio in the tau split-luciferase complementation assay. The strains that seed more efficiently are associated with reduced growth of aggregate-positive cells. See Figures S2A and S2B for data indicating the correlation between a strain's toxicity, EC_{50}, and inflection point in the seeding assay.

(G) Sedimentation analysis of strains. Lysates were ultracentrifuged and tau as well as a loading control protein (cofilin) were probed in the total, supernatant, and pellet fractions (total = Tot, supernatant = Sup, and pellet = Pel). The blots are representative of biological quadruplicates.

(H) Strains feature the majority of tau in the insoluble fraction. Densitometric analysis of tau in the total, supernatant, and pellet fractions was used to calculate supernatant to total ratios (a higher ratio indicates a smaller proportion of tau in the insoluble pellet). The error bars represent SEM of biological quadruplicates.

(I) Densitometric analyses highlight variation in insoluble tau in the various strains. The error bars represent SEM of biological quadruplicates. See Figure S2C for quantification of tau in the total fractions.

(J) Lack of correlation between insoluble tau and seeding activity as measured by peak seeding ratio. See Figure S2D for data indicating lack of correlation between total tau and seeding.

(K) Lack of correlation between total tau and seeding activity. See Figure S2E for data indicating lack of correlation between total tau and toxicity.

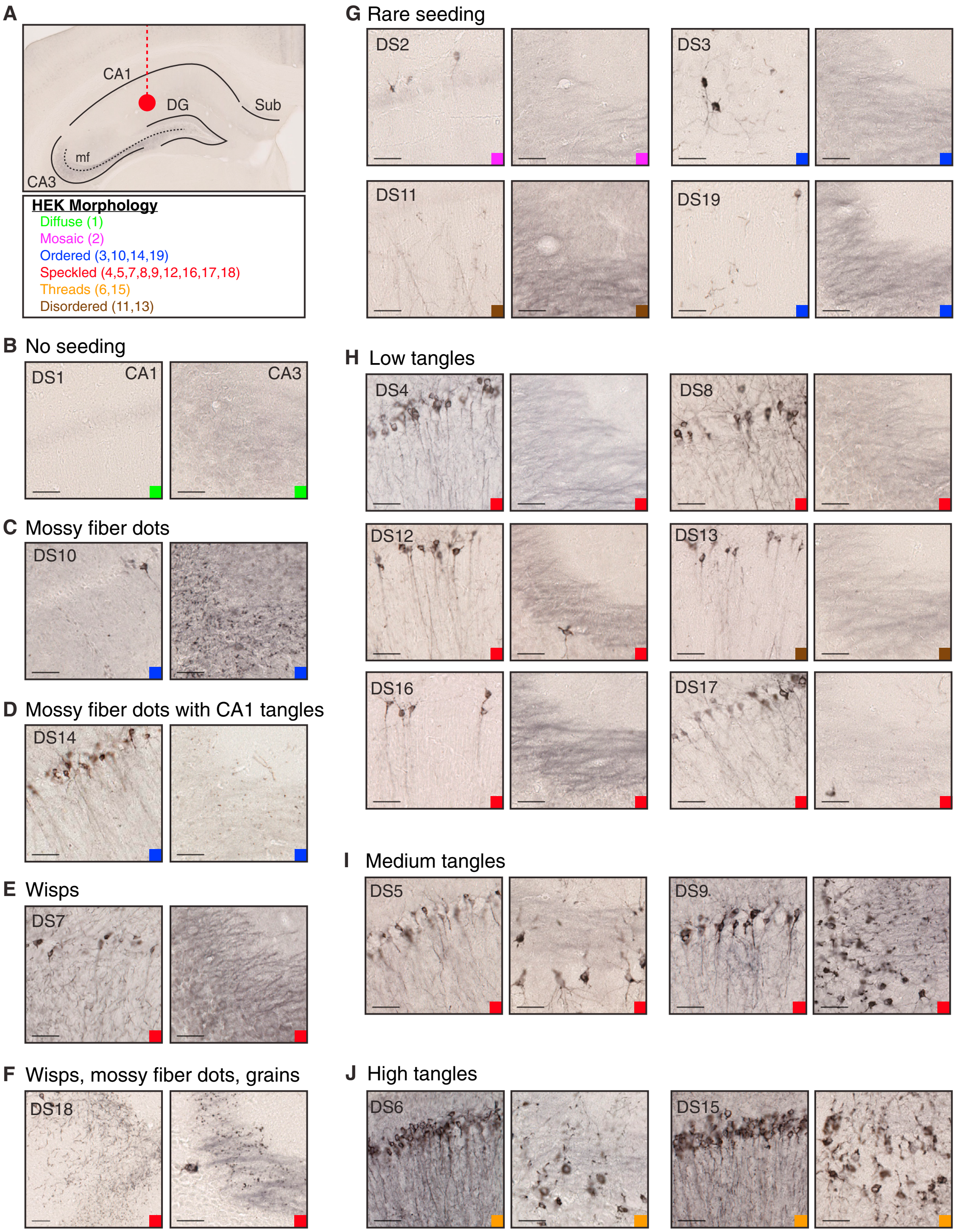

Figure 3. Tau Prion Strains Induce Diverse Patterns of Hippocampal Tau Pathology

(A) Tau strains (10 μg) were injected into the left hippocampus of young PS19 mice (n = 3 per condition, see Table S1). Mouse brains were collected 8 weeks after injection. The relevant regions are indicated on a representative mouse hippocampus (dentate gyrus, DG; mossy fibers, mf; and subiculum, Sub). The HEK morphology table indicates the inclusion patterns in various strains, grouped by text color. The color-coded squares indicate these HEK cell-associated patterns in all images (B–J).

(B) DS1 injection produces no AT8 tau pathology. The representative images of CA1 and CA3 are displayed. The scale bars represent 50 μm. See Figure S3A for whole hippocampal images for DS1–DS19.

(legend continued on next page)

different in terms of their AT8 subcellular localization (soma versus axonal pathology in DS2 and DS11), but this may reflect different levels of maturation of tau aggregates (e.g., pretangles and tangles). Several strains induced low level, yet consistent, tangle-like pathology in CA1 of the hippocampus (DS4, DS8, DS12, DS13, DS16, and DS17) (Figures 3H and S3A). Strains with the highest seeding activity in culture (DS5, DS6, DS9, and DS15) caused widespread tangle-like tau pathology throughout several hippocampal regions (Figures 3I and 3J). Pathology from these robust strains spread to distant regions such as the entorhinal cortex (EC) and contralateral hippocampus (Figure S3B).

Several putative strains induced unique pathology in the hippocampus. DS10 typically produced AT8-positive "dots" in the mossy fiber tracts of the ipsilateral and contralateral hippocampus, while mostly sparing CA1 pyramidal neurons (Figures 3C and S3C) as was observed in previous work (Sanders et al., 2014). DS14, which shared the same ordered cellular phenotype as DS10, also produced mossy fiber dots (Figure 3D). However, this strain showed higher seeding activity in culture and additionally induced CA1 tangle-like pathology in the ipsilateral and contralateral hippocampus (Figure S3C).

DS7 produced "wisps" that resemble neuropil threads (Figure 3E), while inducing weaker AT8 pathology in the main axon branches. This contrasted with several other speckled phenotype strains, which primarily induced AT8 pathology in the main axon (Figures 3H and 3I). DS18 produced wisps, mossy fiber dots, and "grains", which are AT8 positive puncta found throughout the hippocampus (Figure 3F). DS18-inoculated mice also developed grain pathology in the contralateral hippocampus and wisps in the EC, indicating these specific phenotypic features can spread to distant regions (Figure S3D).

Critically, strains with matching limited proteolysis fingerprints produced similar histopathology in vivo (DS3 and 19; DS6 and DS15; and DS12 and DS16) (Figures 3F, 3G, and 3I). These pairs of similar strains (which may propagate identical tau aggregate conformations) displayed similar seeding activity and toxicity levels and induced similar phenotypes in primary neuron culture. Importantly, DS6 and DS15 derive from distinct aggregate sources (aged PS19 mice and recombinant fibrils, respectively), indicating that these strain-based phenotypes are conformation-specific rather than source-specific.

Stability of Distinct Tau Prion Strains

We previously demonstrated that DS9 and DS10 propagate unique conformations and produce identical phenotypes upon reintroduction into DS1 cells. To test whether other strains meet these same criteria for stable prion strains (Sanders et al., 2014), we transduced cell lysate from strains with distinct cellular morphology, seeding activity, and/or in vivo phenotypes into naive DS1 cells (DS1, DS4, DS6, DS7, DS9, DS10, or DS11). We first performed a blinded analysis of cell morphology from a polyclonal population at 5 and 8 days after transduction. The original DS1 and secondary polyclonal DS1 cell lines contained no aggregate-positive cells (Figures S2F–S2H). Blinded counts of DS4, DS7, and DS9 demonstrated the polyclonal population maintained the nuclear speckled phenotype, while DS10 and DS11 secondary lines were readily scored as ordered and disordered. DS6 threads that project from a large juxtanuclear aggregate are only readily apparent when assessing morphology on a population level rather than within individual cells. However, transduction of this cell line reliably induced overt "threads" in the vast majority of secondary cells at 5 days after transduction. By 8 days, tau aggregates in DS6 secondary cells appeared to mature, and the cellular morphology and blinded scoring results resembled that of the original DS6 cell line (Figures S2F–S2H).

To further examine the stability of each strain phenotype, monoclonal secondary cell lines that stably propagate aggregates were isolated by unbiased single-cell sorting at 4 days after transduction of DS4, DS6, DS7, DS9, DS10, and DS11 into the LM1 cell line. Secondary strains displayed the same cellular morphology as the original cell lines (Figure S7A). We tested the seeding activity of each secondary cell line compared to the original strains by transducing cell lysate into a biosensor cell line that expresses tau RD(P301S)-CFP/YFP and quantifying FRET by flow cytometry (Holmes et al., 2014). Secondary cell lines produced seeding activity similar to their respective source strain (Figure S7C). Thus, these are stable strains that induce unique cellular phenotypes even upon serial passage in culture.

Specific Strains Reliably Induce Astrocytic Pathology

Several tauopathies, including CBD and PSP, feature unique glial cell pathology (Kovacs, 2015). While the mechanisms that underlie these patterns are not known, previous work suggested that inoculation of CBD patient lysate into PS19 mice is sufficient to

(C) DS10 produces AT8 positive mossy fiber dot pathology, with limited CA1 pathology as observed previously (Sanders et al., 2014). See Figure S3C for contralateral mf pathology.

(D) DS14 seeds mossy fiber dots similar to DS10, as well as tangle-like pathology, indicating that it is a distinct strain despite its other similar features to DS10. See Figure S3C for contralateral mossy fiber and CA1 pathology.

(E) DS7 induces wisps that resemble neuropil threads, but may fall within axon terminals and the dendritic tree of pyramidal neurons.

(F) DS18 pathology includes wisps and mossy fiber dots similar to DS7 and DS10, respectively, as well as grains that are found throughout much of the hippocampus. See Figure S3D for data indicating that these phenotypes spread to distant synaptically connected locations including the entorhinal cortex.

(G–J) Several strains produce different levels of tangle-like AT8 pathology in CA1 and CA3 of the hippocampus.

(G) DS2, DS3, DS11, and DS19 induce rare AT8 pathology in pyramidal CA1 neurons. The localization of AT8 staining varies in certain cases (cell body versus axonal pathology in DS2 and DS11, respectively).

(H) DS4, DS8, DS12, DS13, DS16, and DS17 induce slightly stronger tangle-like pathology in CA1 of the hippocampus ("low tangles"). CA3 shows limited or no tangle pathology at this time point.

(I) DS5 and DS9 produces AT8 tangle-like tau pathology that reaches CA3 of the hippocampus as well as CA1 pyramidal cells ("medium tangles"). Tangles appear relatively consolidated within the soma of neurons. See Figure S3B for spread of tau pathology to the contralateral hippocampus and ipsilateral EC.

(J) DS6 and DS15 display the highest level of tangle-like AT8 pathology ("high tangles"). Highly consolidated pathology was observed throughout cell bodies and axons of CA1 and CA3 neurons. See Figure S3B for spread of tau pathology to the contralateral hippocampus and ipsilateral EC.

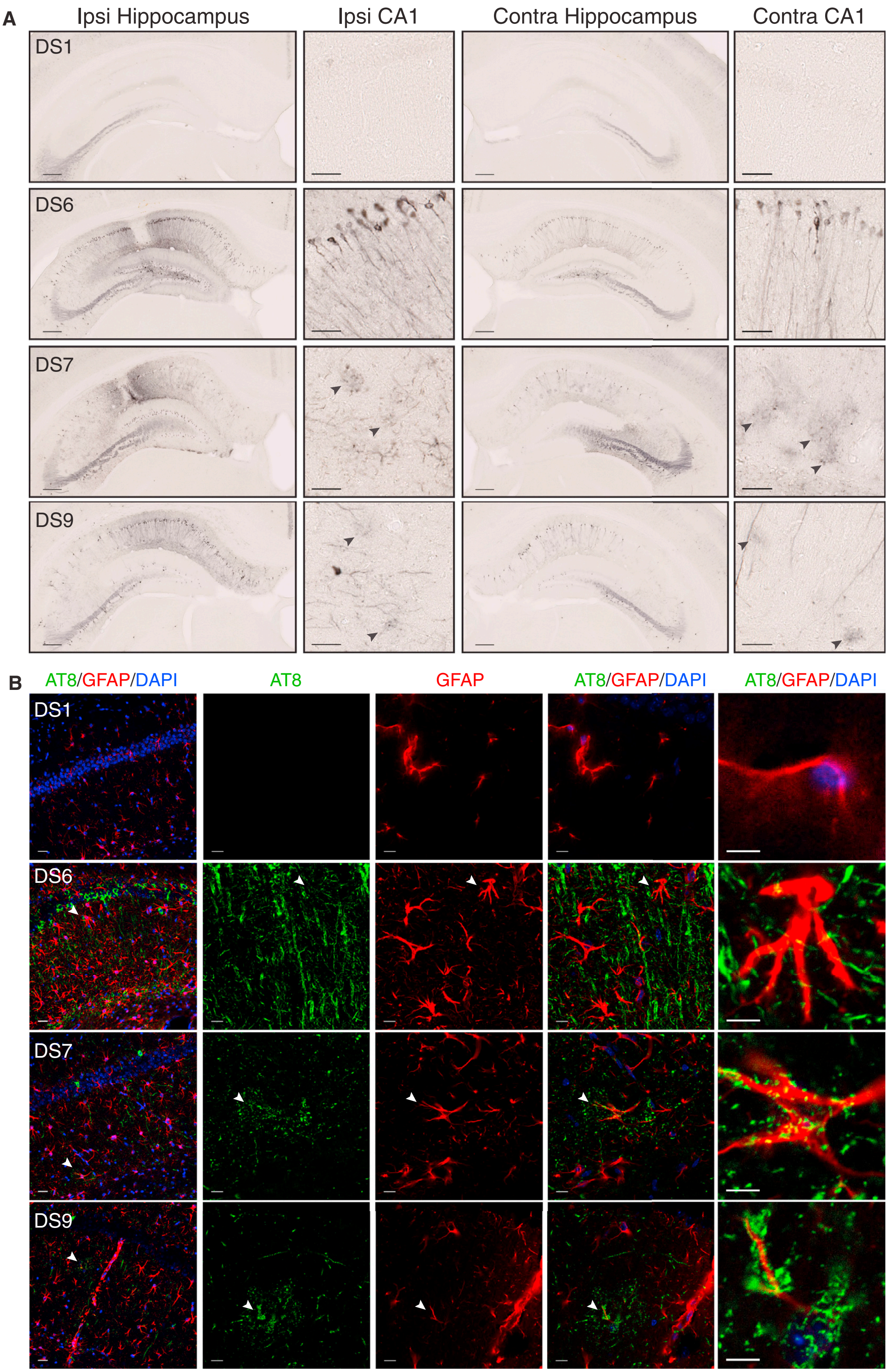

(legend on next page)

induce astrocytic pathology (Boluda et al., 2015). Interpretation of this result was limited by the potential for individual patient brains to contain multiple strains (Sanders et al., 2014). Further, two different paradigms were used for purification of AD versus CBD derived tau, which might also have affected the observed phenotypes (Boluda et al., 2015). We thus assessed astrocytic pathology after inoculation with isolated, individual tau strains.

At 8 weeks after inoculation with DS7 and DS9, we observed tau pathology reminiscent of astrocytic plaques in multiple animals, as noted by small AT8-positive inclusions arranged in ring-like structures (Figure 4A) (Yoshida, 2014). Strains that produced higher levels of tau pathology such as DS6 did not show similar plaque pathology at this time point (Figure 4A). Co-staining with GFAP and AT8 indicated that these accumulations consist of phospho-tau within or directly adjacent to astrocytes as is typical of astrocytic plaques (Figure 4B) (Yoshida, 2014). DS12, DS15, DS16, and DS18 induced a small degree of astrocytic plaque-like pathology at 8 weeks (Figures S4A and S4B). Given these findings, we retrospectively quantified the number of animals with astrocytic plaque-like pathology after completion of the time course injection experiment described below. DS7 or DS9 inoculations induced astrocytic plaque-like pathology in the majority of inoculated mice by 8 weeks (Figure S4A). In contrast, DS4 and DS6 induced limited plaque pathology by 12 weeks, which was far less robust than the level observed in DS7 and DS9 inoculated animals (Figures S4A and S4C). Thus, this phenotype is likely independent of seeding activity and suggests specific tau conformations preferentially and predictably induce astrocytic tau pathology.

While two CBD-derived strains showed a small degree of astrocytic plaque-like pathology (DS12 and DS16), they were sparse at this time point (Figures S4A and S4B). We examined mice inoculated with DS12 and DS16 at 6 months after injection and observed increased levels of astrocytic pathology (Figure S4D). This suggests these two CBD-derived strains produce robust astrocytic plaque pathology after an extended incubation period compared to DS7 or DS9. DS11 and DS13, which were also isolated from CBD patients, did not induce astroctyic plaque pathology 8 weeks after injection. Individual CBD patients likely have multiple tau strains present in their brains (Sanders et al., 2014), which may give rise to the overall pattern of histopathology observed in patients. Alternatively, DS11 and DS13 may simply require more time to produce robust astrocytic plaque pathology in this mouse model, as was observed for DS12 and DS16 (Figures S4B and S4D).

Regional Vulnerability to Specific Strains

Tauopathies feature accumulation of tau pathology in distinct brain regions (Arnold et al., 2013), yet the mechanisms that underlie these patterns are not well understood. To test whether strains differentially induce pathology in specific brain regions, we inoculated DS1, DS4, DS6, DS7, DS9, DS10, or DS11 into six locations per mouse: sensory cortex (SC), caudate/putamen (CP), visual cortex (VC), hippocampus (Hip), thalamus (Thal), and inferior colliculus (IC) (Figure 5A). We chose these strains based on their unique limited proteolysis patterns, different tau pathology induced in the hippocampus, and their low (DS7 and DS11), medium (DS4 and DS10), or high (DS6 and DS9) seeding activity in culture. Further, DS4 and DS11 derive from AD and CBD brain homogenates, respectively. Patients with these diseases have different patterns of tau deposition (Arnold et al., 2013).

After 5 weeks, we quantified the level of AT8 pathology these strains induced at each injection site in a blinded fashion (Figure 5B). All produced hippocampal pathology consistent with the previous injection paradigm, illustrating the reproducibility of these phenotypes (Figure 5C). Strains with the strongest seeding activity in culture (DS6 and DS9) produced pathology in every injected region. DS4, a medium-seeding strain, induced moderate pathology in each region except the IC. DS11 pathology was entirely limited to the hippocampus (Figures 5B and 5C).

DS10 again induced pathology specific to the mossy fiber tracts of the hippocampus (Figure S5A), with limited pathology in the caudate/putamen and thalamus. Of note, it did not produce any pathology in the injected cortical regions. In contrast, DS7 produced limited AT8 pathology in each targeted brain region (Figures 5B and 5C). The specificity of DS10, despite its strong seeding activity, and promiscuity of DS7, despite its weak seeding activity (Figures 1D–1G), were remarkable. These studies indicate tropism of certain strains for specific brain regions (mossy fiber tracts, cortical structures, and IC) that is independent of simple metrics such as seeding activity.

Strains Induce Different Rates of Spread of Tau Pathology along Neuronal Networks

Even within a single clinical syndrome, tauopathy patients experience rapid or slow rates of progression (Armstrong et al., 2014; Thalhauser and Komarova, 2012). PrP strains show different lag phases and rates of neurodegeneration in animal models of prion diseases (Collinge and Clarke, 2007), suggesting this phenomenon may be linked to specific aggregate conformations. While several factors may contribute to the rate of degeneration observed in tauopathy patients, rapid spread of tau pathology likely accelerates this process. Thus, we tested the relationship between strain characteristics and rates of spread of tau pathology.

To control for differences in insoluble material, we first quantified the insoluble tau present in lysate from DS1, DS4, DS6, DS7, DS9, and DS10 prepared for this time course experiment. As

Figure 4. Specific Strains Induce Astrocytic Tau Pathology

(A) AT8 tau pathology 8 weeks after injection with DS1, DS6, DS7, or DS9. DS1 does not induce tau pathology. DS6, DS7, and DS9 develop strong AT8 staining in ipsilateral and contralateral hippocampi. DS7 and DS9 develop diffuse, circular-shaped accumulations of AT8 staining that do not appear to localize to a neuronal cell body (black arrow heads). The scale bars represent 250 μm for the whole hippocampus and 50 μm for CA1.

(B) Co-staining of AT8 (green) for phospho-tau, GFAP (red) for astrocytes, and DAPI (blue) for cell nuclei. DS1 shows limited GFAP staining and no AT8 pathology. DS6 shows strong AT8 staining with limited overlap of AT8 staining. DS7 and DS9 injected mice display astrocytic plaque-like pathology that either deposits within or around GFAP-positive processes of astrocytes. The scale bars represent 25 μm for left column and 10 μm for all remaining images. For further quantification and representative images of other strains that display limited astrocytic plaque pathology, see Figure S4.

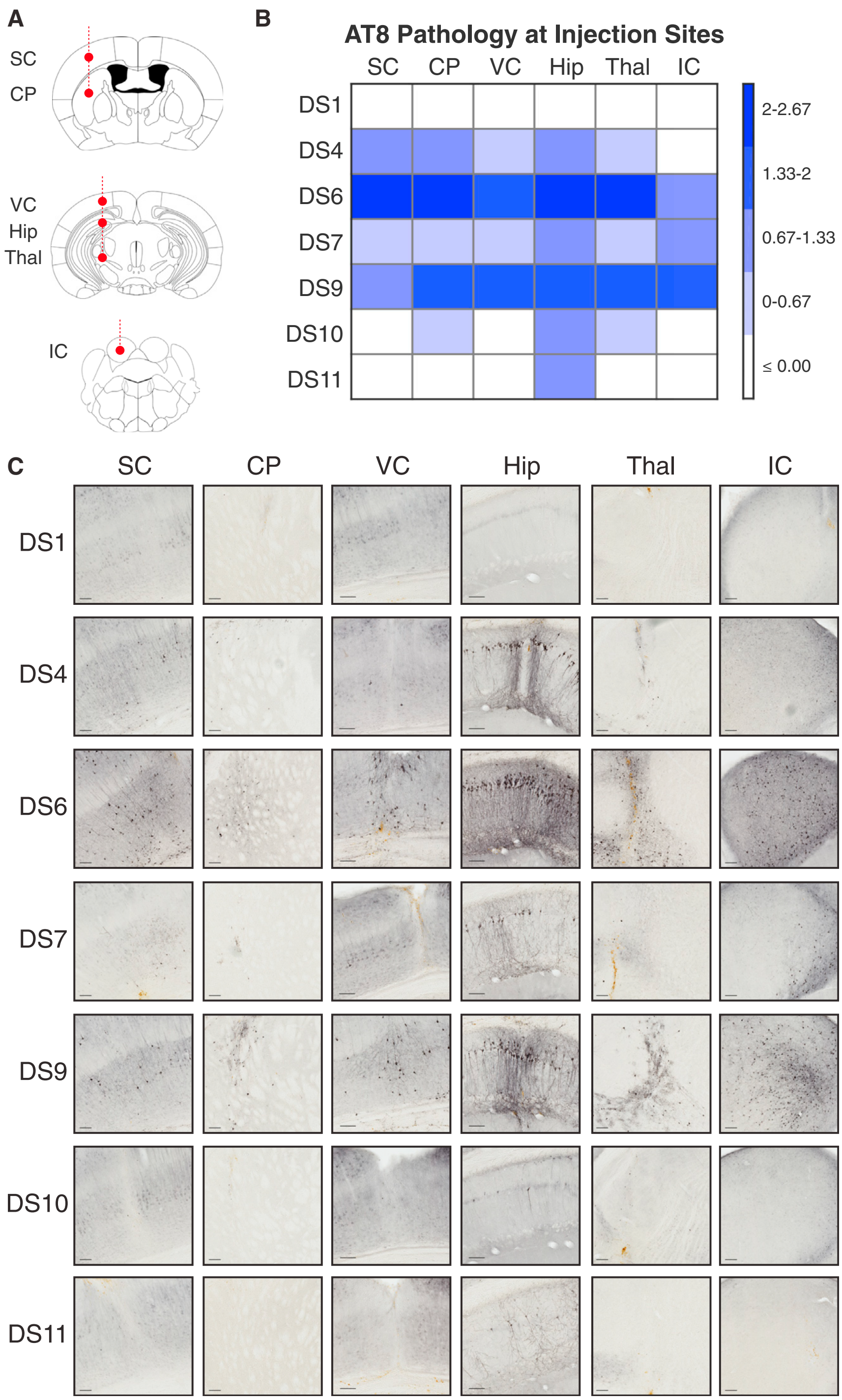

Figure 5. Tau Strains Preferentially Seed Pathology in Specific Brain Regions

(A) Six tau strains were injected simultaneously into six brain regions: SC; CP; VC; Hip; Thal; and IC (5 μg per region). The mice that received DS1 (negative control), DS4, DS6, DS7, DS9, DS10, or DS11 strain injections were kept for 5 weeks post-inoculation before assessment of AT8 tau pathology (n = 3 per condition).

(B) Strains preferentially induced tau pathology in specific brain regions. Slices that contained the injection sites were stained for AT8 phospho-tau. Each injection site was assessed in a blinded fashion for tau pathology on a 0–3 scale (none, low, medium, and high). The level of background AT8 pathology at each injection site was accounted for by subtracting the level of pathology present in DS1 mice within each brain region. A binned heatmap represents the level of pathology observed at the injection site for each strain. Note differences in regional vulnerability.

(C) Representative images are displayed for each brain region injected with the different tau strains. The scale bars represent 100 μm. DS10 mossy fiber pathology is shown in Figure S5A.

expected, each strain contained a large amount of insoluble tau (Figures 6A and 6B). We hypothesized that a strain's ability to seed aggregation of endogenously expressed monomeric tau would primarily determine the rate of spread of pathology. We predicted that strains such as DS6 and DS9 with high seeding activity in culture and in vivo (Figures 1D, 5B, and 5C) would produce rapid spread of pathology even after inoculation of reduced levels of insoluble tau. To test this hypothesis, we included DS6 and DS9 lysate diluted 1:10 as part of this time course experiment.

We injected cell lysate from each condition into the hippocampus of young PS19 mice and collected brains at 4, 8, and 12 weeks post-injection (Figure 6C). While each strain induced tau pathology in the contralateral hippocampus, this occurred at different time points (Figures 6D and 6E). DS6 and DS9 pathology progressed rapidly to the contralateral hippocampus, beginning as early as 4 weeks (Figure 6D). DS10 induced mossy fiber dots and limited CA1 pathology in the ipsilateral and contralateral hippocampus by 8 weeks (Figures 6D and 6E). DS7 wisp pathology also spread to the contralateral hippocampus by 8 weeks (Figure 6D).

While dilution of DS6 and DS9 decreased the initial level of pathology induced upon inoculation, we observed tau pathology in the contralateral hippocampus at 8 weeks. In contrast, DS4 did not show tau pathology in the contralateral hippocampus until 12 weeks (Figures 6D and 6E). Thus, stronger strains induced more rapid spread of pathology even with a reduced amount of insoluble tau inoculum, presumably due to more efficient seeding and spread of endogenous tau aggregates.

While these inoculations induced robust neuronal tau pathology and strain-specific patterns of astrocytic tau pathology, we

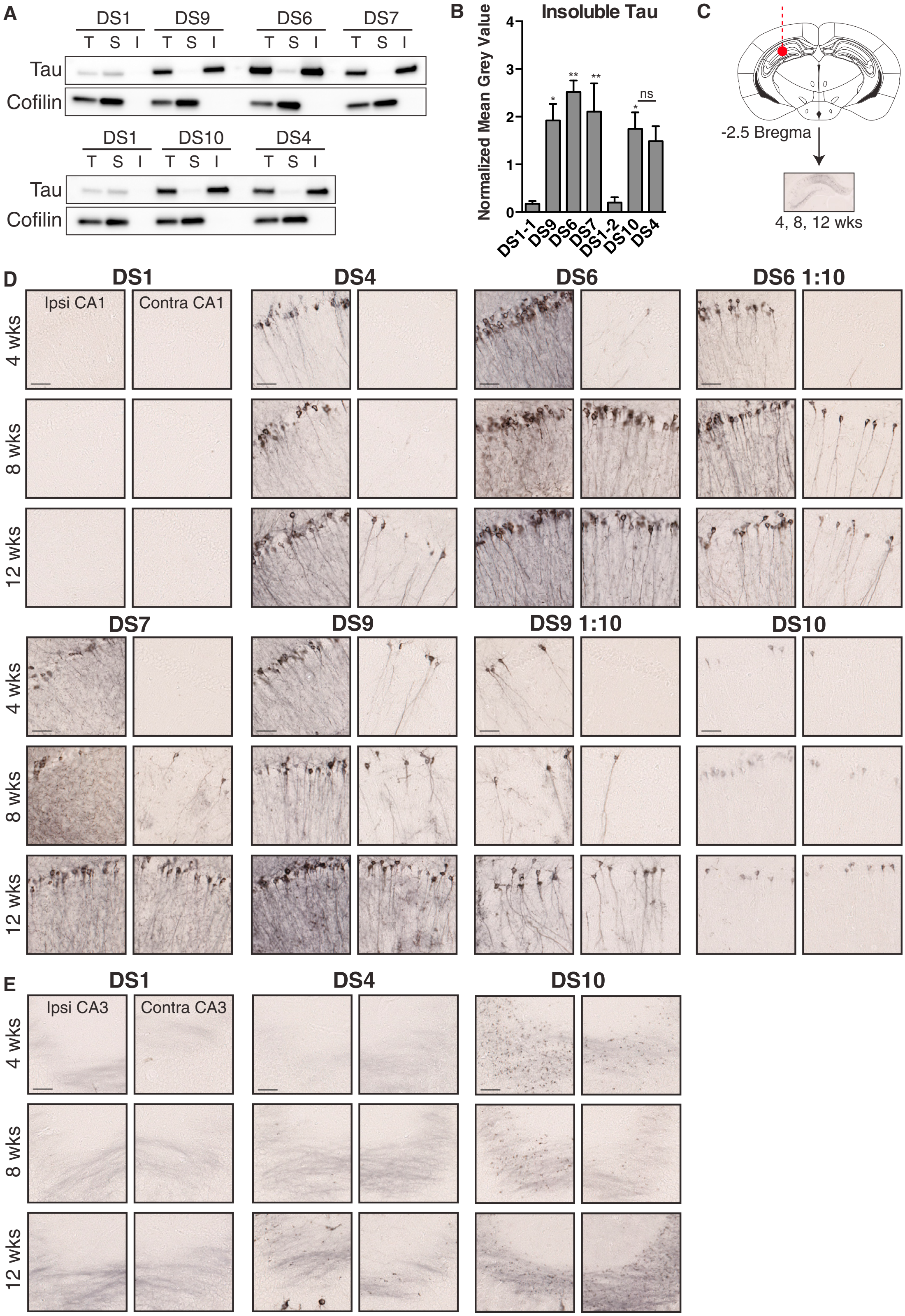

(legend on next page)

did not observe overt neuronal loss at these time points (data not shown). However, to begin to assess the functional effects of distinct strains, we examined the patterns of microglial pathology induced at 12 weeks after inoculation. Compared to DS1 inoculated mice, several strains displayed Iba1-positive rod microglial phenotype, with elongated projections that align along axons of CA1 pyramidal neurons (Figures S6A–S6C). We performed blinded quantification of ramified and rod microglia ipsilateral and contralateral to the site of inoculation. DS6 induced the largest degree of rod microgliosis, while DS7 produced very limited rod microglial pathology. DS4, DS9, and DS10 also produced rod microglia, but we observed this phenotype in the contralateral hippocampus primarily in DS6 and DS10 inoculated mice.

To test the stability of tau strains in vivo, we transduced brain homogenate from the hippocampus of mice at 8 weeks after inoculation into the naive DS1 cell line. DS4, DS6, DS9, and DS10 produced morphologies consistent with the original inoculum (Figures S2F–S2H and S7D). However, brain-derived DS7 produced a mixture of cellular morphologies. This is in contrast to DS7 cell lysate, which stably induces its cellular phenotype in culture, suggesting DS7 may imperfectly template its conformation onto full-length P301S tau in this mouse model.

We isolated monoclonal lines derived from inoculated mouse tissue by transducing brain homogenate into the DS1 line and sorting single aggregate-containing cells. Tau derived from mice inoculated with DS6 strain readily produced thread-containing inclusions in the population of converted cells (Figures S2F and S7D). However, isolation of monoclonal lines was not possible due to toxicity (0/36 individual colonies survived). In contrast, transduction of mouse-derived tissue inoculated with DS7 produced few inclusions in the population overall, with only one resultant monoclonal line. This is consistent with the low seeding activity of the original DS7 line. Multiple secondary lines were derived from brains originally inoculated with DS4, DS9, and DS10 (Figure S7B). FRET-based seeding activity of the secondary cell lines resembled that of the original lines (Figure S7C). Thus, several of these strains stably propagate their phenotype even upon passage through mice.

To assess AT8 pathology induced by each strain, we performed a blinded analysis of AT8 staining in slices at the level of the locus coeruleus, hippocampal injection site, and caudate/putamen. We averaged AT8 pathology rankings for each region and displayed them as a heatmap to visualize the spread of tau pathology (Figure 7A). We subsequently created a limited heatmap for each strain that focuses on specific brain regions, several of which developed pathology over time (Figure 7B). DS10 once again displayed marked neuronal specificity, with strong pathology only in the mossy fiber tracts (Figures 7A and 7B). Blinded analysis also confirmed that DS4 exhibits slower kinetics than DS6 or DS9 even when the latter strains are diluted 10-fold (Figure 7B). DS4 did not develop strong pathology outside the ipsilateral hippocampus until 12 weeks after injection, while the stronger strains showed AT8 staining in distant brain regions by 8 weeks. DS7 induced robust pathology at the injection site as observed previously (Figures 3 and 5). However, the spread of DS7 pathology was relatively slow and appeared limited to the hippocampus (Figures 7A and 7B).

DS6 and 9 spread pathology rapidly to specific brain regions after 4 weeks. DS6 strongly targeted the ipsilateral retrosplenial cortex and LC, while DS9 pathology spread most strongly to the ipsilateral entorhinal cortex and thalamus. Despite these initial differences, by 8 weeks the patterns of pathology induced by these strains largely resembled one another (Figure 7B). While diluted lysate of DS6 and DS9 induced lower levels of pathology at early time points, they induced pathology that spread faster and farther than DS4, DS7, or DS10 and followed similar patterns to that of undiluted DS6 and DS9 lysate (Figure 7B).

We next performed a seeding assay on tissue from the ipsilateral and contralateral hippocampus, thalamus, and sensory cortex at 8 weeks after injection as a second metric of tau pathology. We transduced homogenized brain regions into the FRET biosensor cell line (Holmes et al., 2014) and quantified seeding after 2 days in culture. We have observed that all seeding activity measured after inoculation of DS9 into the hippocampus of tau knockout mice completely dissipates by approximately 6 weeks (data not shown), which suggests any signal identified at this time point likely derives from induced aggregation of endogenous tau expressed in this mouse line.

Several strains displayed robust seeding in the ipsilateral hippocampus (DS4, DS6, DS9, DS10, and 1:10 diluted DS6 and

Figure 6. Strains Induce Different Rates of Tau Pathology Spread

(A) Sedimentation analysis was performed on cell lysate used for the time course inoculation experiment. Each strain contains a large amount of insoluble material (total, T; soluble, S; and insoluble, I). Western blot analysis of insoluble tau was performed on three biological replicates. For each experiment, the soluble fraction was loaded at 2× the concentration of the total and insoluble fractions. A cofilin loading control was performed on the blots to verify the same amount of cell lysate was added for each strain.

(B) The level of insoluble tau present in each strain was quantified by measuring the mean gray value of the insoluble tau western blot band. The samples were normalized to the mean gray value of cofilin in the total cell lysate fraction. DS1-1 and DS1-2 represent biological replicates of DS1. ANOVA shows strains have significantly more insoluble tau than DS1. A two-way t test demonstrates DS10 and DS4 do not contain significantly different levels of insoluble tau (ns for $p > 0.5$; * for $p \leq 0.05$; and ** for $p \leq 0.01$). The error bars represent SEM of biological triplicates.

(C) Strains were inoculated into the hippocampus of young PS19 mice (n = 5–6 per condition per time point, see Table S1). DS6 and DS9 lysate diluted 1:10 in HEK293 cell lysate were also injected (n = 4–5 per condition per time point). The mice were collected at 4, 8, or 12 weeks.

(D) Representative images of ipsilateral and contralateral CA1 are displayed for each strain at 4, 8, and 12 weeks post-injection. AT8-positive tau pathology spreads to the contralateral hippocampus at different time points. The diluted DS6 and DS9 lysate show faster spread than concentrated DS4 and more robust spread than DS7 and DS10 at 8 weeks post-injection. The scale bars represent 50 μm. See Figure S6 for data regarding strain-specific rod microglial phenotype present at 12 weeks after inoculation.

(E) Spread of mossy fiber dot pathology occurs by 8 weeks in DS10 mice. The dot pathology appears eventually to develop in DS4 mice, but spread appears delayed compared to DS10.

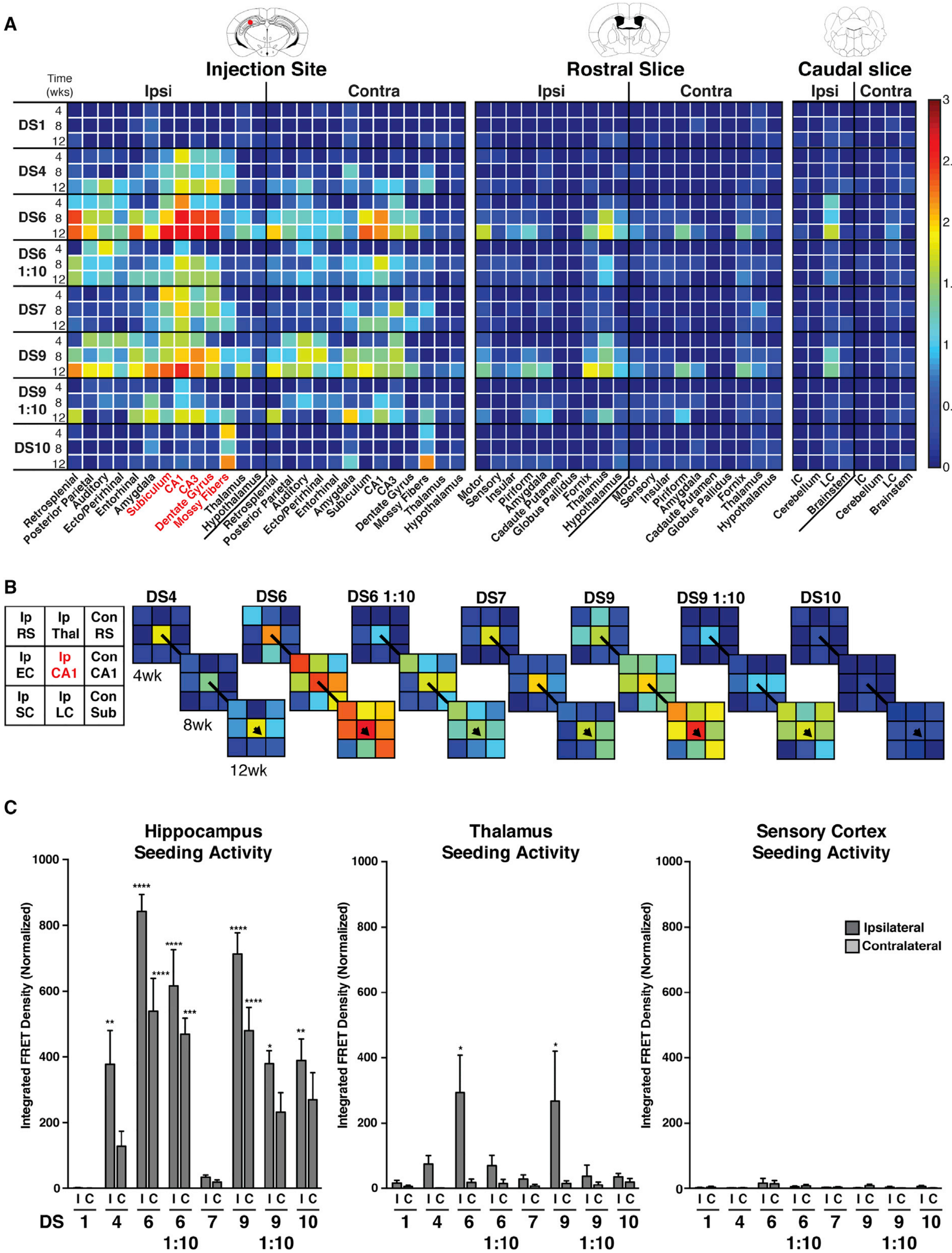

(legend on next page)

DS9). While each of these strains spread to the contralateral hippocampus, DS4 showed distinctly less contralateral seeding activity as a percentage of the ipsilateral hippocampus (Figure 7C). Further, DS6 and DS9 showed variable yet significant seeding activity in the ipsilateral thalamus. The level of seeding observed in DS1 inoculated mice is consistent with the level observed in this mouse model at 4–5 months of age, suggesting this signal is due to spontaneous aggregation of endogenous tau that normally occurs within this model (Holmes et al., 2014). DS7 showed remarkably low seeding activity, while DS10 induced relatively robust seeding from the hippocampus despite only inducing mossy fiber AT8 tau pathology (Figures 6E and 7C). This is consistent with the seeding activity for the original inoculum as observed by the split-luciferase assay (Figures 1D and 2G–2I). These results are also consistent with the different rates of spread observed by AT8 immunohistochemistry for DS4 versus DS6 and DS9, while providing a separate metric to quantify the spread of pathology for strains such as DS10.

DISCUSSION

Overview of Findings

We have tested whether specific tau prion strains can account for critical neuropathological features that are used to discriminate tauopathies. We characterized strains by various biochemical and biological metrics, including inclusion morphology, seeding activity in dividing cells and primary neurons, detergent solubility, cellular toxicity, limited proteolysis, and reintroduction into reporter cells. We inoculated all 18 strains individually into the hippocampi of a transgenic tauopathy mouse model, causing distinct patterns of tau pathology in cell bodies, axons, and dendrites. To test for regional vulnerability, we injected six strains into six different brain regions and waited 5 weeks to evaluate pathology. Many induced pathology in all regions (DS6, DS7, and DS9), while others exhibited restricted patterns in which very little or no pathology occurred despite direct exposure of neurons to a particular strain (DS4, DS10, and DS11). We next tested whether strains exhibited unique rates of propagation through the brain. In this case, we observed correlations with in vitro parameters: strains with high seeding activity tended to spread more rapidly through the brain, with one important exception—strain DS10—which only spread to the contralateral mossy fiber tracts of the hippocampus. These observations suggest that distinct tau prion strains could account for many of the features observed in human tauopathies.

Limitations of this Experimental Approach

It is impossible at this time to directly control tau strain production in vivo using transgenic mice or to propagate strains faithfully and indefinitely in vitro without using cultured cells. This work relies on a cell model that expresses a truncated form of tau with a fluorescent protein tag, an imperfect system that has nonetheless allowed us to propagate distinct tau prion strains indefinitely. Likewise, in mice, we utilized a model that expresses full-length human tau (1N4R) that contains a disease-associated mutation (P301S) (Yoshiyama et al., 2007). While this obviously deviates from sporadic tauopathy that occurs in most individuals, it has enabled us to rapidly and reliably induce unique tau pathology based on local inoculation. We cannot exclude the possibility that inoculated tau prions themselves are moving throughout the brain and inducing pathology based on local uptake rather than true trans-neuronal propagation (Rey et al., 2013). Nonetheless, our observations suggest a fundamental disease mechanism whereby strain-specific differences govern seeding, propagation, and specific regional vulnerability.

The Utility of Studying Isolated Strains

Our prior work has indicated that human tauopathy brains, even those carefully defined by histopathology, exhibit enormously diverse strain content within and between individuals (Sanders et al., 2014). Thus syndromes that appear to be clinically and neuropathologically identical are potentially quite distinct in terms of their strain composition. This presents obvious challenges when attempting to define strains present in human disease based principally on inoculation of purified aggregates into mice. Fibril preparations created in vitro also exhibit tremendous conformational heterogeneity, as clearly illustrated by studies of α-synuclein in which one dominant fibril structure shifts to another upon serial seeding reactions (Guo et al., 2013). In this work, we have stably propagated strains with specific biochemical properties in a simple culture system based on expression of tau RD-YFP. While technical limitations have restricted our ability to define the specific structures of tau aggregates present in these strains, this work suggests a single dominant structure is faithfully propagated in each line. This has enabled us to make predictions about phenotypes in vivo based on properties observed in vitro.

Figure 7. Strain Dictates the Rate and Pattern of Spread of Tau Pathology

(A) Slices from mice injected with each strain at each time point were stained for AT8 pathology. Tau pathology was quantified in a blinded fashion on a 0–3 scale and averaged for each location within a given condition (n = 5–6 per condition). A continuous heatmap was generated. Note differential rates of spread and regional vulnerability. The regions are listed on the x axis and conditions/time points are on the y axis.

(B) Limited heatmaps were generated from the above data set (Figure 7A). Ipsilateral (Ip) and contralateral (Con) regions were included to assess patterns and rates of spread of pathology (retrosplenial cortex, RS; EC; SC; Thal; CA1 of hippocampus, CA1; locus coruleus, LC; and subiculum, Sub). Time points are arranged in order from earliest (4 weeks) to latest (12 weeks). Diluted DS6 and DS9 lysates are also displayed (DS6 1:10 and DS9 1:10).

(C) Homogenized tissue from the hippocampus, thalamus, or sensory cortex of mice 8 weeks after inoculation with strains was applied to tau biosensor cell lines. After 48 hr, cells were collected and flow cytometry was performed to quantify the level of seeding activity in each region by integrated FRET density (percent FRET-positive cells*median fluorescent intensity of FRET positive cells = IFD) (Holmes et al., 2014). DS4 induces lower spread of seeding activity to the contralateral hippocampus at 8 weeks. DS10 induces high seeding activity despite limited AT8 pathology, while DS7 induces low seeding activity despite high AT8 pathology. DS6 and DS9 also induce seeding activity in the ipsilateral thalamus. A one-way ANOVA with Bonferroni correction for multiple comparisons was performed between ipsilateral DS1 and every other sample within a given region (*p $\leq$ 0.05; **p $\leq$ 0.01; ***p $\leq$ 0.001; and ****p $\leq$ 0.0001). The error bars represent SEM, n = 4–5. See Figure S7 for data regarding secondary cell line isolation of strains derived from inoculated mice or strain cell lysate.

Prion Strains Characterized In Vitro

PrP prion strains have distinct, yet reproducible patterns of incubation time, neuropathology, and behavioral phenotypes (Collinge and Clarke, 2007). Strains are presumably distinct amyloid structures that faithfully replicate in a living system and produce well-defined pathology. Thus, if a strain is identified, it is possible to predict incubation time and resultant pathology (Collinge and Clarke, 2007). In this work, we characterized multiple tau strains from recombinant, mouse, and patient sources in vitro and in vivo. Their detailed characterization in vitro using several metrics (inclusion morphology, solubility, seeding efficiency, and limited proteolysis) allowed us to make predictions regarding their effects in vivo. For instance, DS6 and DS9 induced robust spread of tau pathology even upon dilution, which was predicted by in vitro seeding activity. Importantly, while seeding activity correlated best with induction of local and distant pathology, this is an imperfect metric. For example, DS10 inoculation produces very limited pathology in vivo despite its relatively strong seeding activity in vitro. This indicates a major influence of other as yet unidentified strain-specific parameters. With further, more detailed study, we hope to link specific structural characteristics to various steps in pathogenesis, i.e., to define the ''logic'' that predicts biological effects. For instance, cell-type specificity (or at least preference) might be based on differential strain binding affinities to heparan sulfate proteoglycans (Holmes et al., 2013). Likewise, post-translational modifications of monomeric tau within a target cell might render it more or less vulnerable to conversion by a specific strain.

Distinct Cellular Pathologies In Vivo

Tauopathies are defined histopathologically by several criteria, especially the pattern of intracellular tau accumulation: neurofibrillary tangles, Pick bodies, threads, grains, axonal puncta, etc. (Kovacs, 2015). Although we have readily observed patterns of pathology reminiscent of those described in patients, we have not attempted to link human patterns of pathology to those in P301S mice, which express only a single isoform of mutant tau. Instead, we wish to emphasize how conformational differences in tau prion strains are sufficient to create an enormous pathological diversity: neurofibrillary tangles, soma versus axonal accumulation, grain-like structures, dendritic and axonal terminal deposits that resemble threads, and astrocytic plaques.

The presence or absence of specific glial pathology also contributes to the definition of tauopathies (Yoshida, 2014). We observed that certain strains produce AT8-postive pathology in patterns reminiscent of astrocytic plaques described in tauopathies, with localization of phospho-tau inclusions along the processes of GFAP-positive astrocytes (Yoshida, 2014). We cannot attribute these effects to tau seeding activity or toxicity, as we observed these phenomena in DS7 (low seeding and low toxicity) and DS9 (high seeding and high toxicity). Distinct strains also induced different levels of rod microglial pathology.

Given that inoculates were identical with the exception of tau structure, and the transgenic mouse model expresses only a single tau isoform, we conclude that tau prion strains themselves dictate the resultant glial pathology. Further, three strain pairs (DS3/DS19; DS12/DS16; and DS6/DS15) that displayed similar biochemical features and limited proteolysis patterns produced similar patterns of neuropathology in vivo. These strains served to internally validate the methods we developed and highlight the close relationship of strain type to induced pathology.

Rates of Propagation In Vivo

Neurodegenerative diseases progress at different rates for unknown reasons. Similar to previous observations regarding PrP prion strains (Legname et al., 2006), our data indicate that the characteristics of an individual tau prion strain are sufficient to dictate the rate at which pathology spreads throughout the nervous system. Seeding activity correlates with this phenomenon, but cannot completely explain it. Instead, the rate of spread appears to reflect a unique interaction of specific strains with vulnerable cells. For example, strain DS10 seeds very strongly in vitro, but fails to propagate pathology outside of the hippocampal mossy fibers. Likewise, DS6 seeds very strongly in vitro, but exhibits a longer lag phase as it spreads to specific brain regions such as the entorhinal cortex versus the retrosplenial cortex. In contrast, DS9 showed more rapid spread to the entorhinal than the retrosplenial cortex. Taken together, our results suggest that the rate of propagation must be strongly influenced by raw seeding potential, i.e., the ability to convert monomeric tau upon direct introduction to the cytoplasm via lipofectamine, but also the ability of a given strain to spontaneously enter and replicate within a vulnerable cell.

Distinct Regional Vulnerabilities

Regional or ''selective'' neuronal vulnerability in neurodegenerative diseases has long mystified investigators. PrP prion strains appear to account for differential regional involvement of the brain (Collinge and Clarke, 2007). Within the limits of our experimental system, our identification and characterization of distinct tau strains has allowed us to test whether aggregate structure itself defines regional vulnerability. We have found striking strain-specific regional differences, both in the pattern of spread from a single hippocampal inoculum and also in vulnerability to a direct injection. These effects correlated with individual tau strains, independent of an inoculum dose that could have accounted for vulnerability. For example, 10-fold dilution of a potent strain, DS9, produced patterns of spreading pathology very similar to a full dose. Further, low-dose DS9 spread at a faster rate than a full dose of DS4, even though the initial ''seed burden'' of DS9 was less. By contrast, strain DS10 has relatively high seeding activity, yet it selectively targets the mossy fibers of the hippocampus and does not convert tau in several other brain regions even after direct inoculation.

Others previously observed that different tau fibril preparations produce unique patterns of pathology based on inoculation of tau purified from tauopathy brains or crude homogenates (Boluda et al., 2015; Clavaguera et al., 2013), and two groups have inoculated unique α-synuclein preparations (Bousset et al., 2013; Guo et al., 2013; Peelaerts et al., 2015). However, no prior studies can attribute these effects to a specific, well-characterized strain or structure and make predictions about the behavior of a strain in vivo from the biochemical properties of that inoculum. Given that we can now link specific pathology patterns to single tau prion strains, the experiments described here should enable new approaches to define how the structural characteristics of prions dictate neuronal vulnerability.

Implications for Diagnosis and Therapy

We propose that tau prion strains will explain the diversity of human neuropathology and will be required for mechanistic understanding of disease. Precise diagnosis of tauopathy now depends on histopathology, yet we have observed different strain composition patterns in putatively identical pathological syndromes (Sanders et al., 2014). Further, diversity and evolution may confound efforts to target a specific strain, as for PrP (Giles et al., 2010; Weissmann et al., 2011). Tau prion strains as defined by their specific conformations should have enormous power to help elucidate the structural determinants that underlie and predict the pathological patterns of diverse human tauopathies and to devise appropriate therapies.

EXPERIMENTAL PROCEDURES

Generation of Monoclonal Strain Library

Cells stably expressing tau RD(P301L/V337M) fused to YFP (DS1) were treated with recombinant tau fibrils or cell/brain homogenate. Resultant monoclonal lines were isolated and analyzed for inclusion morphology, seeding by split luciferase assay, and protease digestion as previously described (Sanders et al., 2014). These analyses identified 18 putatively distinct strains (DS2–DS19).

Limited Proteolysis

Cell lysates (60 μg) in PBS/Triton X-100 were digested with pronase (30 μg/mL) for 1 hr at 37°C, then resolved by SDS-PAGE and western blot probed with primary anti-tau antibody 2B11.

Sedimentation Analysis of Strain Library

Cell lysates were spun at 186,000 × *g* for 60 min. Pellets were washed with 1 mL lysis buffer and spun for an additional 30 min. Samples were resolved by SDS-PAGE and western blot using rabbit polyclonal anti-tau antibody ab64193 (Abcam).

Toxicity and Seeding Assay

LM10 cells, a monoclonal cell line expressing high levels of tau RD(P301L/V337M)-CFP and tau RD(P301L/V337M)-YFP, were transduced with 20 μg of clarified cell lysate. After 72 hr, FRET-positive cells were sorted by FACS (Holmes et al., 2014) and replated. After 7 days, the number of FRET-positive and FRET-negative cells was quantified by flow cytometry.

Animal Maintenance and Inoculation Experiments

PS19 mice expressing 4R1N P301S human tau under the murine prion promoter (Yoshiyama et al., 2007) were used. Strains were inoculated intracerebrally via 10 μL gas-tight Hamilton syringes. All experiments involving animals were approved by the University of Texas Southwestern Medical Center Institutional Animal Care and Use Committee.

Histology and Quantification of AT8 Pathology

50 μm frozen sections were used. For DAB stain, biotinylated AT8 primary antibody (Thermo Scientific) was used. Images of AT8-stained slices were collected via Olympus Nanozoomer 2.0-HT (Hamamatsu). The level of tau pathology present in each region was determined by blinded analysis with a semiquantitative 0–3 scale (no pathology, mild, moderate, and severe). Pathology was averaged among biological replicates and plotted as a heatmap using MATLAB as described.

SUPPLEMENTAL INFORMATION

Supplemental Information includes Supplemental Experimental Procedures, seven figures, and three tables and can be found with this article online at http://dx.doi.org/10.1016/j.neuron.2016.09.055.

AUTHOR CONTRIBUTIONS

S.K.K. designed and performed all in vivo and primary neuron experiments, inoculum sedimentation analysis, secondary cell line isolation and characterization, and brain immunohistochemistry. D.W.S. designed and performed all in vitro cell culture and biochemistry experiments to characterize DS1–DS19. Both authors assisted in data analysis, writing, and figure preparation for this manuscript. T.L.T. provided technical assistance with stereotaxic injections, tissue collection, sectioning, and immunohistochemistry. A.R. conducted blinded scoring of AT8 pathology and microglial pathology. A.M.S. performed limited proteolysis experiments. J.V.-A. assisted with development of primary neuron culture experiments and MATLAB analysis of pathology. T.M.M. provided guidance and reagents for in vivo experiments. M.I.D. provided guidance for in vitro and in vivo experiments and assisted in the writing and preparation of figures for this manuscript.

ACKNOWLEDGMENTS

We thank Ann McKee, Bill Seeley, and Lea Grinberg for providing invaluable reagents for this study. We thank Peter Davies for providing MC1 antibody. We thank Matthew Brier, Jennifer Furman, Brandon Holmes, Suzanne Schindler, and Niall Prendergast for providing guidance and critiques during the preparation of this manuscript. This work was funded by NIH/NIA grant F30AG048653 (S.K.K.); NIH grant F31NS086251 (D.W.S.); NIH/NIA R01AG048678, NIH/NINDS R01NS071835, the Tau Consortium, and the Cure Alzheimer's Fund (M.I.D.). This work was supported by the Hope Center Alafi Neuroimaging Laboratory at Washington University in St. Louis, NeuroModels Facility, Whole Brain Microscopy Facility, Moody Foundation Flow Cytometry Facility, and High Throughput Screening Core at University of Texas Southwestern.

Received: March 22, 2016
Revised: July 22, 2016
Accepted: September 23, 2016
Published: October 27, 2016

REFERENCES

Armstrong, M.J., Castellani, R.J., and Reich, S.G. (2014). "Rapidly" progressive supranuclear palsy. Mov. Disord. Clin. Pract. (Hoboken) *1*, 70–72.

Arnold, S.E., Toledo, J.B., Appleby, D.H., Xie, S.X., Wang, L.-S., Baek, Y., Wolk, D.A., Lee, E.B., Miller, B.L., Lee, V.M.-Y., and Trojanowski, J.Q. (2013). Comparative survey of the topographical distribution of signature molecular lesions in major neurodegenerative diseases. J. Comp. Neurol. *521*, 4339–4355.

Barghorn, S., Zheng-Fischhöfer, Q., Ackmann, M., Biernat, J., von Bergen, M., Mandelkow, E.M., and Mandelkow, E. (2000). Structure, microtubule interactions, and paired helical filament aggregation by tau mutants of frontotemporal dementias. Biochemistry *39*, 11714–11721.

Bessen, R.A., and Marsh, R.F. (1994). Distinct PrP properties suggest the molecular basis of strain variation in transmissible mink encephalopathy. J. Virol. *68*, 7859–7868.

Boluda, S., Iba, M., Zhang, B., Raible, K.M., Lee, V.M.-Y., and Trojanowski, J.Q. (2015). Differential induction and spread of tau pathology in young PS19 tau transgenic mice following intracerebral injections of pathological tau from Alzheimer's disease or corticobasal degeneration brains. Acta Neuropathol. *129*, 221–237.

Bousset, L., Pieri, L., Ruiz-Arlandis, G., Gath, J., Jensen, P.H., Habenstein, B., Madiona, K., Olieric, V., Böckmann, A., Meier, B.H., and Melki, R. (2013).

Structural and functional characterization of two alpha-synuclein strains. Nat. Commun. *4*, 2575.

Braak, H., and Braak, E. (1991). Neuropathological stageing of Alzheimer-related changes. Acta Neuropathol. *82*, 239–259.

Clavaguera, F., Bolmont, T., Crowther, R.A., Abramowski, D., Frank, S., Probst, A., Fraser, G., Stalder, A.K., Beibel, M., Staufenbiel, M., et al. (2009). Transmission and spreading of tauopathy in transgenic mouse brain. Nat. Cell Biol. *11*, 909–913.

Clavaguera, F., Akatsu, H., Fraser, G., Crowther, R.A., Frank, S., Hench, J., Probst, A., Winkler, D.T., Reichwald, J., Staufenbiel, M., et al. (2013). Brain homogenates from human tauopathies induce tau inclusions in mouse brain. Proc. Natl. Acad. Sci. USA *110*, 9535–9540.

Collinge, J., and Clarke, A.R. (2007). A general model of prion strains and their pathogenicity. Science *318*, 930–936.

Collinge, J., Sidle, K.C.L., Meads, J., Ironside, J., and Hill, A.F. (1996). Molecular analysis of prion strain variation and the aetiology of 'new variant' CJD. Nature *383*, 685–690.

de Calignon, A., Polydoro, M., Suárez-Calvet, M., William, C., Adamowicz, D.H., Kopeikina, K.J., Pitstick, R., Sahara, N., Ashe, K.H., Carlson, G.A., et al. (2012). Propagation of tau pathology in a model of early Alzheimer's disease. Neuron *73*, 685–697.

Frost, B., Jacks, R.L., and Diamond, M.I. (2009a). Propagation of tau misfolding from the outside to the inside of a cell. J. Biol. Chem. *284*, 12845–12852.

Frost, B., Ollesch, J., Wille, H., and Diamond, M.I. (2009b). Conformational diversity of wild-type Tau fibrils specified by templated conformation change. J. Biol. Chem. *284*, 3546–3551.

Giles, K., Glidden, D.V., Patel, S., Korth, C., Groth, D., Lemus, A., DeArmond, S.J., and Prusiner, S.B. (2010). Human prion strain selection in transgenic mice. Ann. Neurol. *68*, 151–161.

Guo, J.L., and Lee, V.M.-Y. (2011). Seeding of normal Tau by pathological Tau conformers drives pathogenesis of Alzheimer-like tangles. J. Biol. Chem. *286*, 15317–15331.

Guo, J.L., Covell, D.J., Daniels, J.P., Iba, M., Stieber, A., Zhang, B., Riddle, D.M., Kwong, L.K., Xu, Y., Trojanowski, J.Q., and Lee, V.M. (2013). Distinct α-synuclein strains differentially promote tau inclusions in neurons. Cell *154*, 103–117.

Holmes, B.B., DeVos, S.L., Kfoury, N., Li, M., Jacks, R., Yanamandra, K., Ouidja, M.O., Brodsky, F.M., Marasa, J., Bagchi, D.P., et al. (2013). Heparan sulfate proteoglycans mediate internalization and propagation of specific proteopathic seeds. Proc. Natl. Acad. Sci. USA *110*, E3138–E3147.

Holmes, B.B., Furman, J.L., Mahan, T.E., Yamasaki, T.R., Mirbaha, H., Eades, W.C., Belaygorod, L., Cairns, N.J., Holtzman, D.M., and Diamond, M.I. (2014). Proteopathic tau seeding predicts tauopathy in vivo. Proc. Natl. Acad. Sci. USA *111*, E4376–E4385.

Hutton, M., Lendon, C.L., Rizzu, P., Baker, M., Froelich, S., Houlden, H., Pickering-Brown, S., Chakraverty, S., Isaacs, A., Grover, A., et al. (1998). Association of missense and 5′-splice-site mutations in tau with the inherited dementia FTDP-17. Nature *393*, 702–705.

Iba, M., Guo, J.L., McBride, J.D., Zhang, B., Trojanowski, J.Q., and Lee, V.M.-Y. (2013). Synthetic tau fibrils mediate transmission of neurofibrillary tangles in a transgenic mouse model of Alzheimer's-like tauopathy. J. Neurosci. *33*, 1024–1037.

Knowles, T.P.J., Vendruscolo, M., and Dobson, C.M. (2014). The amyloid state and its association with protein misfolding diseases. Nat. Rev. Mol. Cell Biol. *15*, 384–396.

Kovacs, G.G. (2015). Invited review: Neuropathology of tauopathies: principles and practice. Neuropathol. Appl. Neurobiol. *41*, 3–23.

Lee, V.M., Goedert, M., and Trojanowski, J.Q. (2001). Neurodegenerative tauopathies. Annu. Rev. Neurosci. *24*, 1121–1159.

Legname, G., Nguyen, H.-O.B., Peretz, D., Cohen, F.E., DeArmond, S.J., and Prusiner, S.B. (2006). Continuum of prion protein structures enciphers a multitude of prion isolate-specified phenotypes. Proc. Natl. Acad. Sci. USA *103*, 19105–19110.

Liu, L., Drouet, V., Wu, J.W., Witter, M.P., Small, S.A., Clelland, C., and Duff, K. (2012). Trans-synaptic spread of tau pathology in vivo. PLoS ONE *7*, e31302.

Mirbaha, H., Holmes, B.B., Sanders, D.W., Bieschke, J., and Diamond, M.I. (2015). Tau trimers are the minimal propagation unit spontaneously internalized to seed intracellular aggregation. J. Biol. Chem. *290*, 14893–14903.

Nonaka, T., Watanabe, S.T., Iwatsubo, T., and Hasegawa, M. (2010). Seeded aggregation and toxicity of alpha-synuclein and tau: cellular models of neurodegenerative diseases. J. Biol. Chem. *285*, 34885–34898.

Peelaerts, W., Bousset, L., Van der Perren, A., Moskalyuk, A., Pulizzi, R., Giugliano, M., Van den Haute, C., Melki, R., and Baekelandt, V. (2015). α-Synuclein strains cause distinct synucleinopathies after local and systemic administration. Nature *522*, 340–344.

Prusiner, S.B. (1998). Prions. Proc. Natl. Acad. Sci. USA *95*, 13363–13383.

Raj, A., Kuceyeski, A., and Weiner, M. (2012). A network diffusion model of disease progression in dementia. Neuron *73*, 1204–1215.

Rey, N.L., Petit, G.H., Bousset, L., Melki, R., and Brundin, P. (2013). Transfer of human α-synuclein from the olfactory bulb to interconnected brain regions in mice. Acta Neuropathol. *126*, 555–573.

Sanders, D.W., Kaufman, S.K., DeVos, S.L., Sharma, A.M., Mirbaha, H., Li, A., Barker, S.J., Foley, A.C., Thorpe, J.R., Serpell, L.C., et al. (2014). Distinct tau prion strains propagate in cells and mice and define different tauopathies. Neuron *82*, 1271–1288.

Sanders, D.W., Kaufman, S.K., Holmes, B.B., and Diamond, M.I. (2016). Prions and protein assemblies that convey biological information in health and disease. Neuron *89*, 433–448.

Thalhauser, C.J., and Komarova, N.L. (2012). Alzheimer's disease: rapid and slow progression. J. R. Soc. Interface *9*, 119–126.

Walker, L.C., and Jucker, M. (2015). Neurodegenerative diseases: expanding the prion concept. Annu. Rev. Neurosci. *38*, 87–103.

Weissmann, C., Li, J., Mahal, S.P., and Browning, S. (2011). Prions on the move. EMBO Rep. *12*, 1109–1117.

Yoshida, M. (2014). Astrocytic inclusions in progressive supranuclear palsy and corticobasal degeneration. Neuropathology *34*, 555–570.

Yoshiyama, Y., Higuchi, M., Zhang, B., Huang, S.-M., Iwata, N., Saido, T.C., Maeda, J., Suhara, T., Trojanowski, J.Q., and Lee, V.M.-Y. (2007). Synapse loss and microglial activation precede tangles in a P301S tauopathy mouse model. Neuron *53*, 337–351.

Zhou, J., Gennatas, E.D., Kramer, J.H., Miller, B.L., and Seeley, W.W. (2012). Predicting regional neurodegeneration from the healthy brain functional connectome. Neuron *73*, 1216–1227.

Neuron, Volume *92*

Supplemental Information

Tau Prion Strains Dictate Patterns of Cell Pathology, Progression Rate, and Regional Vulnerability In Vivo

Sarah K. Kaufman, David W. Sanders, Talitha L. Thomas, Allison J. Ruchinskas, Jaime Vaquer-Alicea, Apurwa M. Sharma, Timothy M. Miller, and Marc I. Diamond

Supplemental Figure Legends

Figure S1, related to Figure 1. Origin of strains and primary neuron seeding
(A) Diverse sources of aggregated tau were used to derive 18 putative tau strains in a monoclonal HEK293 cell line (Clone 1/DS1). Strains were derived from different recombinant protein, transgenic mouse, and patient sources as indicated in the table. Some strains were passaged from previously characterized cell lines. Strains are color-coded based on their associated inclusion morphology.

(B) Limited proteolysis of DS1, 4, 6, 7, 9, 10 and 11 demonstrates the digestion patterns are stable even upon dilution with HEK lysate. Strain lysate diluted 1:1 with HEK lysate is indicated with a D.

(C) Strains showed variability in their ability to seed the formation of insoluble tau aggregates in primary hippocampal neurons expressing full-length 1N4R tau(P301S)-YFP. Lysates from individual strains were added to primary neurons. Eleven days later, neurons were fixed with Triton X-100 extraction of soluble material. Accumulation of conformationally altered tau was assessed by MC1 staining (red). Strong seeders in the tau split-luciferase complementation assay produced more insoluble tau pathology in neurons. Scale bars = 50 μm for the wide view and 10 μm for the inset images.

A

Strain (DS)	Morphology	Origin of Inoculate	Passaged Line From Sanders et al. (2014)
1	Diffuse	None	Clone 1
2	Mosaic	AGD Cell Line	AGD2 (Mosaic)
3	Ordered	Rec Fibrils	N/A
4	Speckles	AD Brain Homogenate	N/A
5	Speckles	Rec Fibrils	N/A
6	Threads	P301S Mouse Homogenate	N/A
7	Speckles	Rec Fibrils	N/A
8	Speckles	P301S Mouse Homogenate	N/A
9	Speckles	Rec Fibrils	Clone 9
10	Ordered	Rec Fibrils	Clone 10
11	Disordered	CBD Cell Line	CBD3 (Disordered)
12	Speckles	CBD Cell Line	CBD3 (Speckles)
13	Disordered	CBD Cell Line	CBD5 (Disordered)
14	Ordered	Rec Fibrils	N/A
15	Threads	Rec Fibrils	N/A
16	Speckles	CBD Cell Line	CBD3 (Speckles)
17	Speckles	AD Cell Line	AD1 (Speckles)
18	Speckles	CTE Brain Homogenate	N/A
19	Ordered	Rec Fibrils	N/A

Abbreviations:
Rec fibrils = recombinant tau fibrils
AGD = argyrophilic grain disease
AD = Alzheimer's disease
CBD = corticobasal degeneration
CTE = chronic traumatic encephalopathy

B

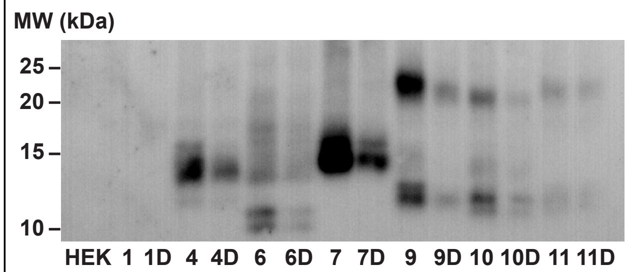

C

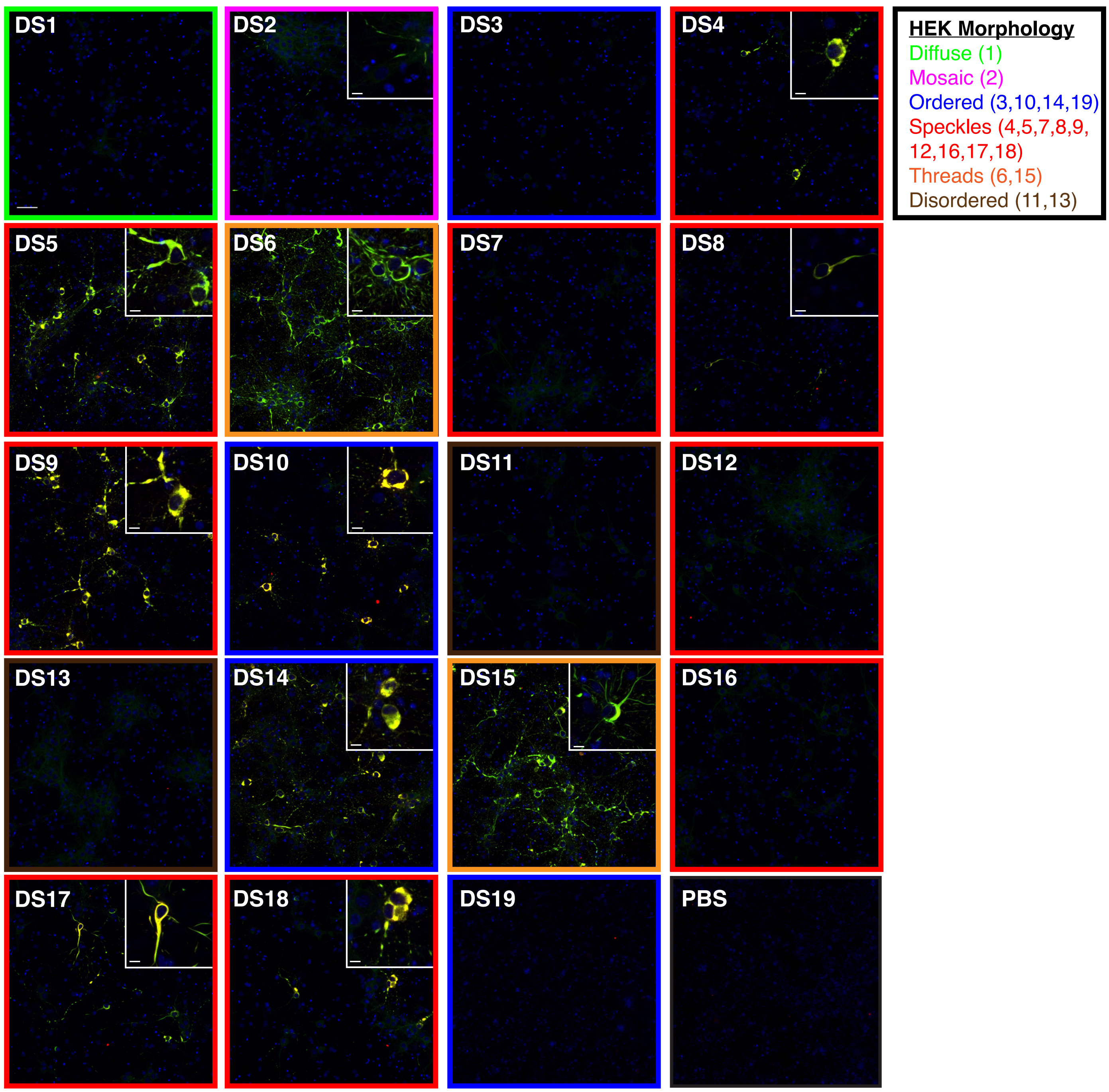

Figure S2, related to Figure 2. Seeding activity but not total tau correlates with toxicity *in vitro*

(A) Strain seeding activity correlates with toxicity. The number of aggregate-positive (FRET+) cells for a strain was plotted against its associated EC_{50} in the tau split-luciferase complementation assay. Strains that reached their half-maximal seeding at lower protein concentrations were associated with decreased cell growth.

(B) A significant correlation exists between cell growth (FRET+ cells) and seeding inflection point (the amount of lysate required for a strain to show significant seeding in the tau split-luciferase complementation assay).

(C) Densitometric analysis of tau in the total fractions suggests variability in the extent of total tau in the various strains. Error bars represent S.E.M. of biological quadruplicates.

(D) Total tau does not correlate with a strain's peak seeding ratio.

(E) No correlation was observed between a strain's total tau and its toxicity as assessed by relative growth of aggregate-positive (FRET+) cells.

(F) Normalized, blinded counts of strain morphology for DS1, 4, 6, 7, 9, 10, 11, 5 days and 8 days after transduction into the naïve DS1 cell line. Strains were classified as threads, ordered, disordered, or speckled as described in the methods.

(G) Representative images used for quantitation of the original strains and secondary polyclonal strains at 5 and 8 days post-transduction.

(H) Enlarged images of the original and transduced strains.

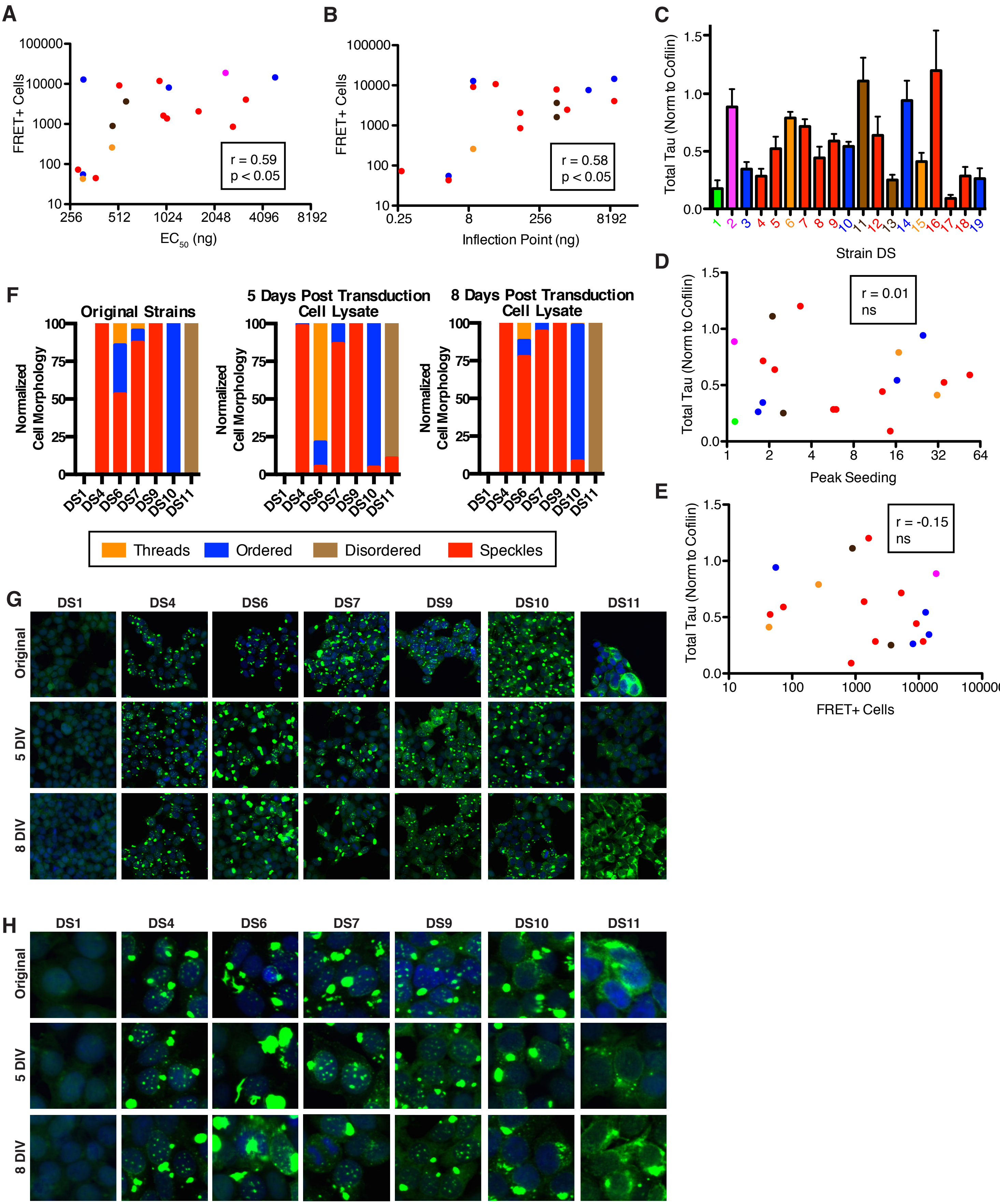
A
B
C
D
E
F
G
H
FRET+ Cells
EC50 (ng)
r = 0.59
p < 0.05
Inflection Point (ng)
r = 0.58
p < 0.05
Total Tau (Norm to Cofilin)
Strain DS
Peak Seeding
r = 0.01
ns
r = -0.15
ns
Original Strains
5 Days Post Transduction Cell Lysate
8 Days Post Transduction Cell Lysate
Normalized Cell Morphology
Threads
Ordered
Disordered
Speckles
DS1
DS4
DS6
DS7
DS9
DS10
DS11
Original
5 DIV
8 DIV

Figure S3, related to Figure 3. Strains induce unique tau pathology in various brain regions
(A) AT8 pathology present in the ipsilateral hippocampus of DS1-19. HEK Morphology refers to the inclusion appearance in HEK cells of strains inoculated into the hippocampus. Scale bars = 250 μm.

(B) Spread of AT8 tau pathology to the contralateral hippocampus and ipsilateral entorhinal cortex in DS5 and 9 (medium tangles), and DS6 and 15 (high tangles). Low levels of DS1 baseline staining can be observed in the ipsilateral EC, and is at the level expected for animals at this age. Scale bars = 250 μm for the whole hippocampus, and 50 μm for EC.

(C) DS10 and 14 show mossy fiber dots in the contralateral hippocampus. DS14 CA1 AT8 tangle-like pathology is much stronger than DS10. Scale bars = 250 μm for the whole hippocampus, and 50 μm for CA1 and CA3.

(D) DS18 shows grains throughout CA1, and wisps in the ipsilateral EC, showing the unique features induced by this strain can spread to distant regions. Scale bars = 250 μm for the whole hippocampus, and 50 μm for CA1 and EC.

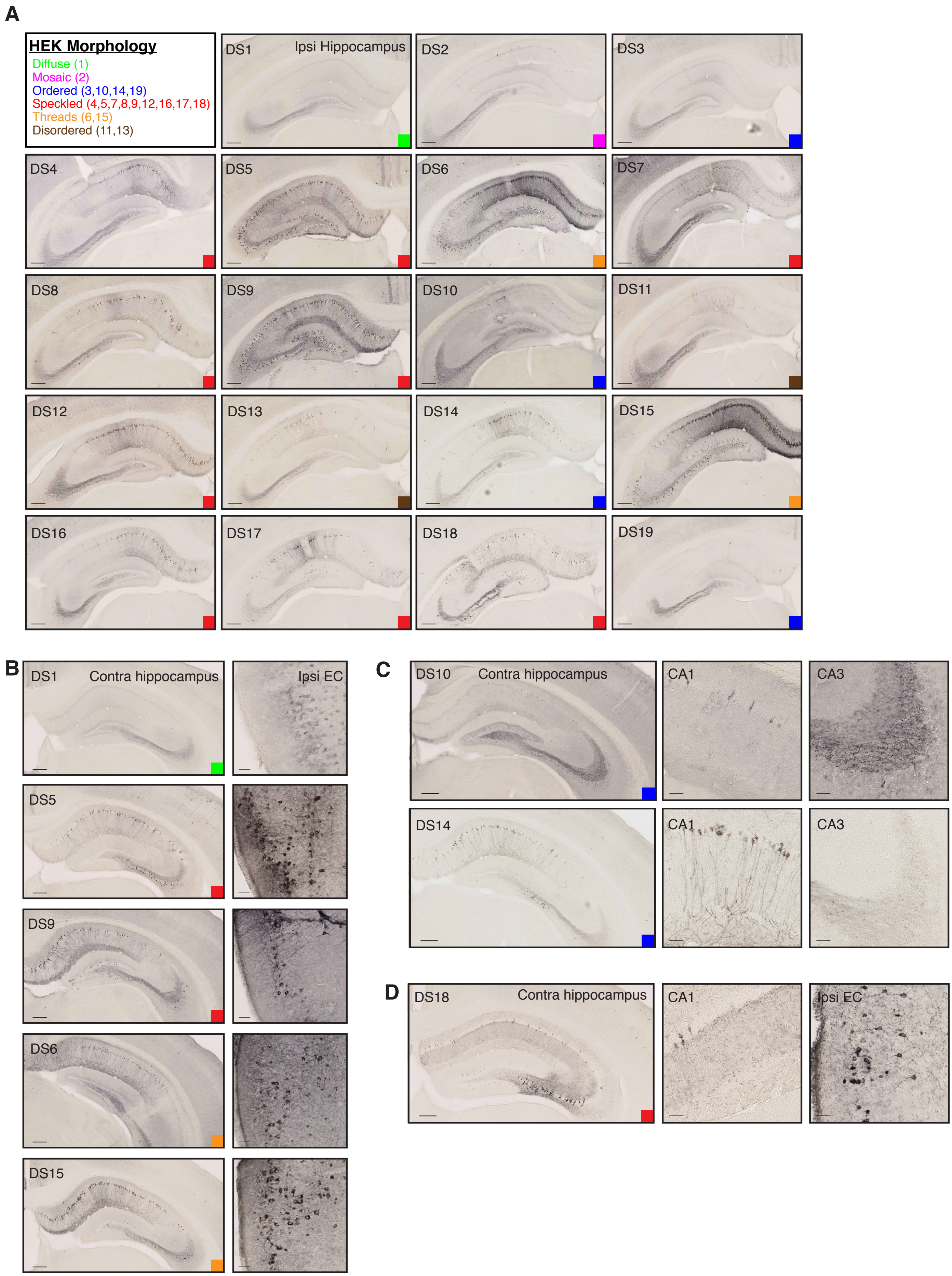
A
HEK Morphology
Diffuse (1)
Mosaic (2)
Ordered (3,10,14,19)
Speckled (4,5,7,8,9,12,16,17,18)
Threads (6,15)
Disordered (11,13)
DS1
Ipsi Hippocampus
DS2
DS3
DS4
DS5
DS6
DS7
DS8
DS9
DS10
DS11
DS12
DS13
DS14
DS15
DS16
DS17
DS18
DS19
B
DS1
Contra hippocampus
Ipsi EC
DS5
DS9
DS6
DS15
C
DS10
Contra hippocampus
CA1
CA3
DS14
CA1
CA3
D
DS18
Contra hippocampus
CA1
Ipsi EC

Figure S4, related to Figure 4. Certain strains reliably produce robust astrocytic pathology that increases over time.
(A) Quantification of the number of mice that displayed astrocytic tau pathology at 4, 8, or 12 weeks post-inoculation with different strains. Two experimental inoculations were assessed for astrocytic pathology (for strain panel and time course experiments, see **Supplemental Table 1 and 2**). Greater than 85% of animals inoculated with DS7 or 9 display astrocytic plaque-like pathology by 8-weeks. Other strains do not show any consistent plaque pathology until 12 weeks.

(B) Representative images of the astrocytic plaque-like pathology observed in 1/3 animals inoculated with DS12, 15, 16, and 18 at 8 weeks post-injection. Scale bars = 50 μm.

(C) Average number of plaques counted in ipsilateral hippocampus (also see Table S1). Several other strains begin to develop astrocytic pathology by 12 weeks, but the number of plaques is far lower than that observed in DS7 and 9.

(D) Images of age-matched PS19 mouse hippocampus and CA1 region, versus DS9, 12, and 16 inoculated hippocampi at 6 months post-inoculation. DS12 and 16 developed increased levels of astrocytic plaque pathology at this time point. Scale bars = 500um.

A

	Number of animals with astrocytic plaques		
	Weeks post inoculation		
Strain	**4**	**8**	**12**
DS1	0/4	0/10	0/5
DS2	-	0/3	-
DS3	-	0/3	-
DS4	0/4	0/4	4/5
DS6	0/5	0/6	4/6
DS6 1:10	0/5	1/4	3/4
DS7	0/5	7/8	6/6
DS9	2/5	6/7	6/6
DS9 1:10	3/4	4/4	4/4
DS10	0/5	0/5	0/6
DS11	-	0/3	-
DS12	-	1/3	-
DS13	-	0/3	-
DS14	-	0/3	-
DS15	-	2/3	-
DS16	-	1/3	-
DS17	-	0/3	-
DS18	-	1/3	-
DS19	-	0/3	-

B

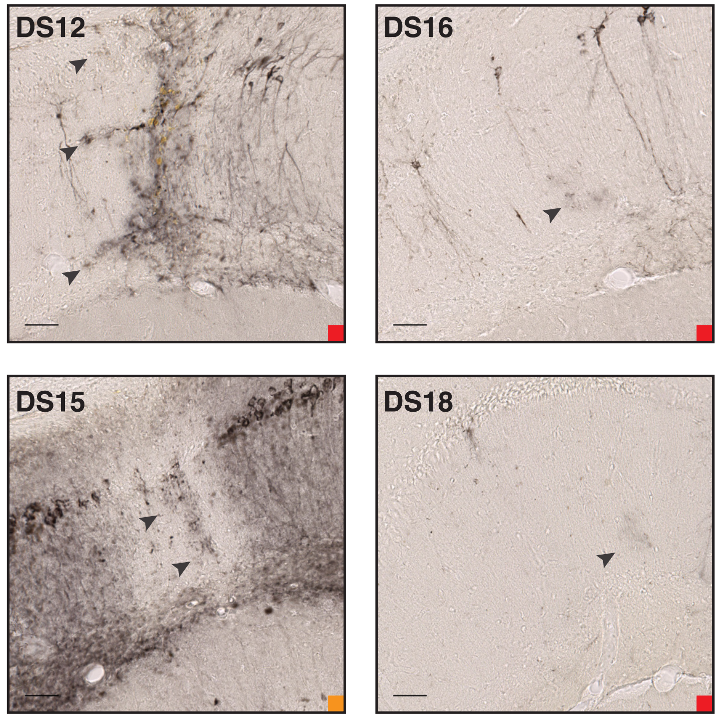

C

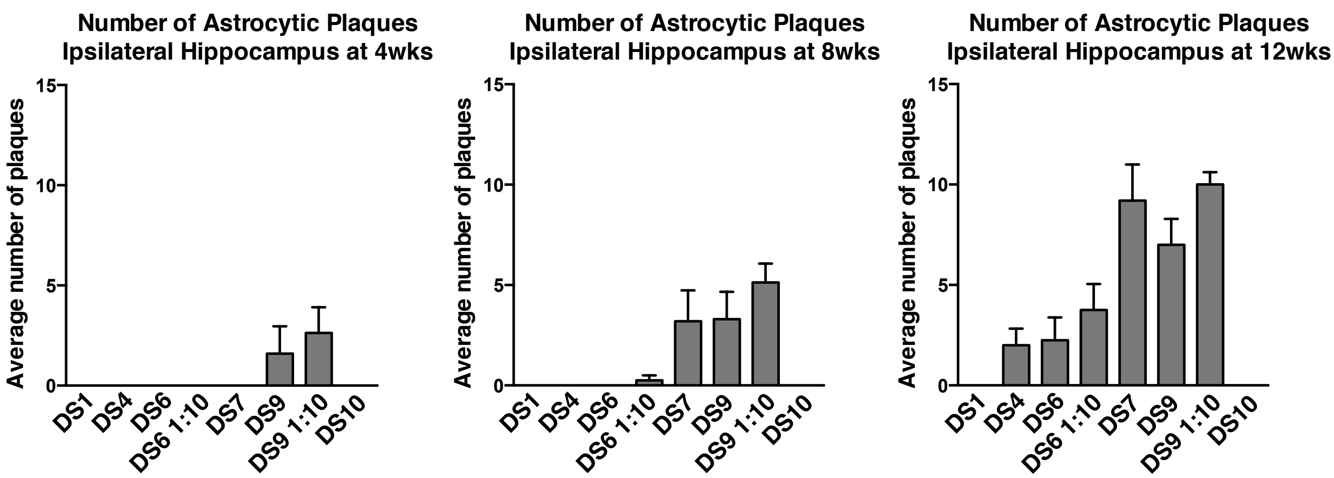

D

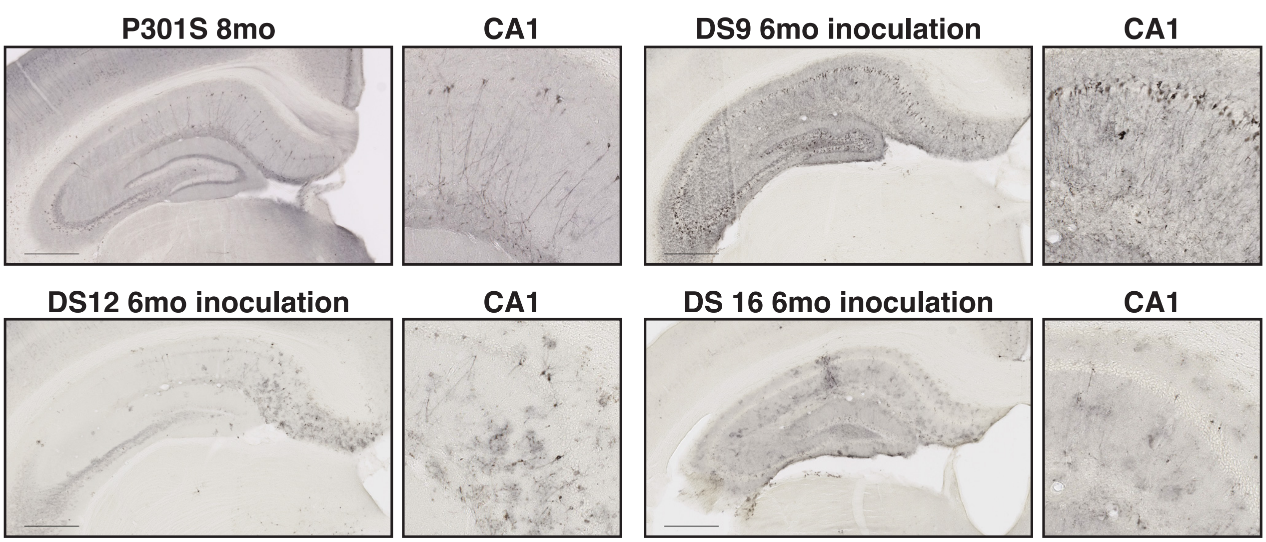

Figure S5, related to Figure 5. DS10 reliably produces mossy fiber dot pathology
(A) Mice inoculated with DS10 for the regional vulnerability experiments develop mossy fiber dots as expected in the ipsilateral and contralateral hippocampus. Scale bars = 250 μm for the whole hippocampus, and 50 μm for CA3.

A

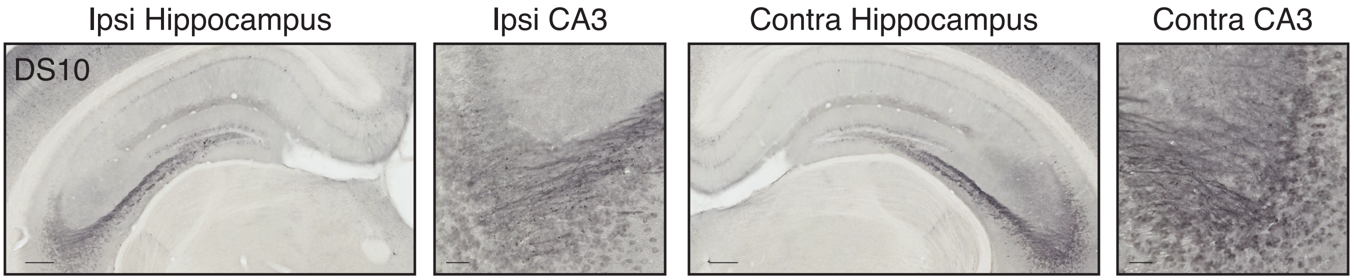
Ipsi Hippocampus
Ipsi CA3
Contra Hippocampus
Contra CA3
DS10

Figure S6, related to Figure 6. Strain Specific Microglial Phenotypes

(A) Ramified and rod microglia were quantified in the ipsilateral and contralateral hippocampus at 12 weeks post-inoculation.

(B) Rod microglia are significantly increased in all strains except DS7 in the ipsilateral hippocampus, but only in DS6 and 10 in the contralateral hippocampus. (* for $P \leq 0.05$; ** for $P \leq 0.01$; *** for $P \leq 0.001$; **** for $P \leq 0.0001$).

(C) Representative images of microglial pathology in mice 12 weeks post-inoculation. The rod microglial phenotype is apparent in several images (white arrowheads).

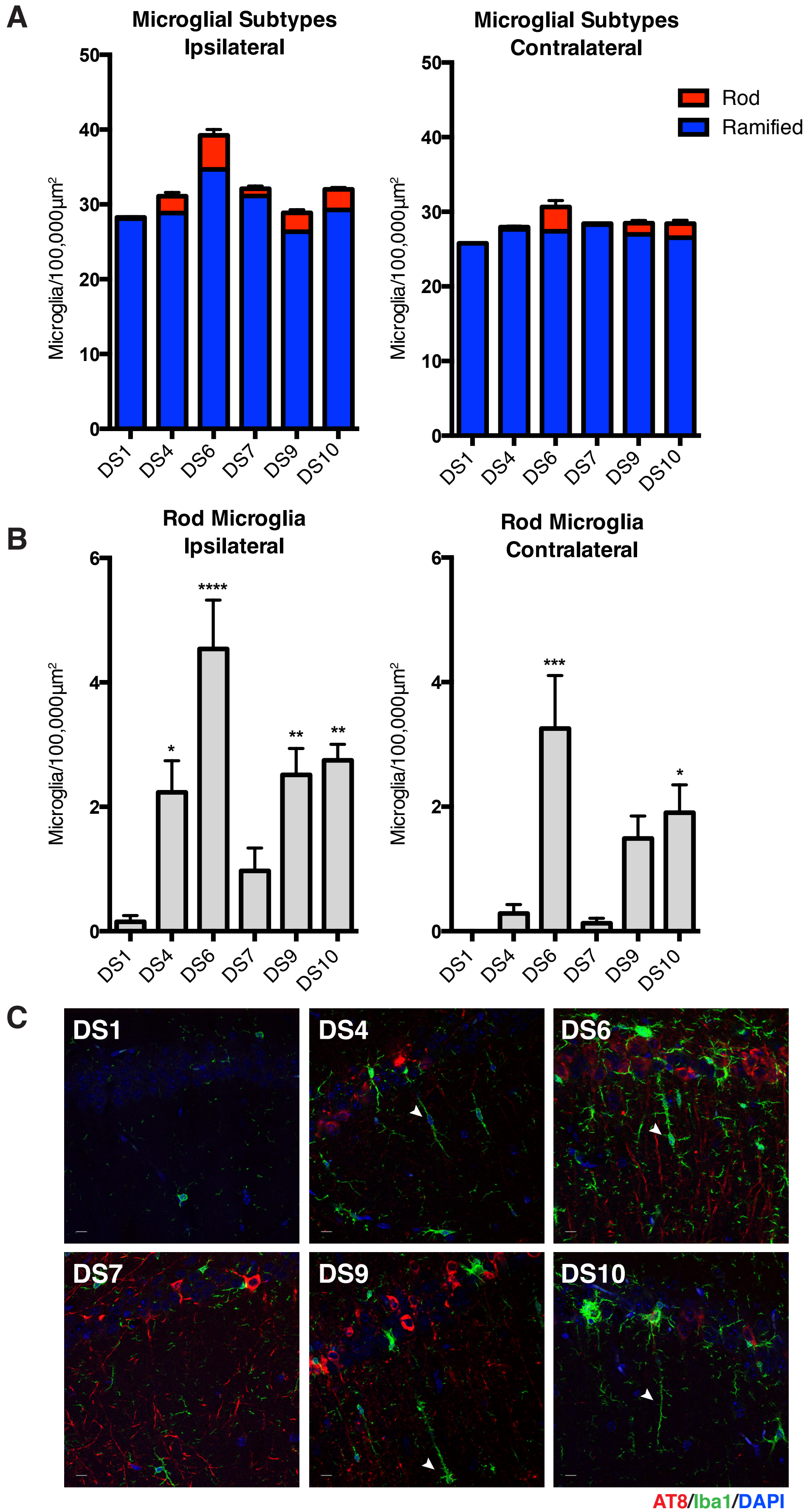
A
Microglial Subtypes
Ipsilateral
Microglial Subtypes
Contralateral
Rod
Ramified
Microglia/100,000µm²
50
40
30
20
10
0
DS1
DS4
DS6
DS7
DS9
DS10
B
Rod Microglia
Ipsilateral
Rod Microglia
Contralateral
6
4
2
0
*
****
**
**
***
*
C
DS1
DS4
DS6
DS7
DS9
DS10
AT8/Iba1/DAPI

Figure S7, related to Figure 7. Monoclonal Cell Lines Maintain Original Strain Properties

(A) Representative images of monoclonal cell lines derived after single cell sorting of DS1 cells transduced with DS4, 6, 7, 9, 10, or 11 cell lysate.

(B) Representative images of monoclonal cell lines derived from mouse brain homogenate at 8 weeks post-inoculation of DS4, 7, 9, or 10.

(C) FRET-based seeding of original or secondary cell lines. Student t-tests were used to assess differences in seeding activity between the original and secondary cell lines (two-tailed, ns for $P > 0.05$; N/A if only one secondary cell line was isolated).

(D) Normalized blinded scoring of DS1 cells at 5 days post-transduction of mouse hippocampal homogenate. Transduced samples were from mice at 8 weeks post-inoculation with DS4, 6, 7, 9, or 10.

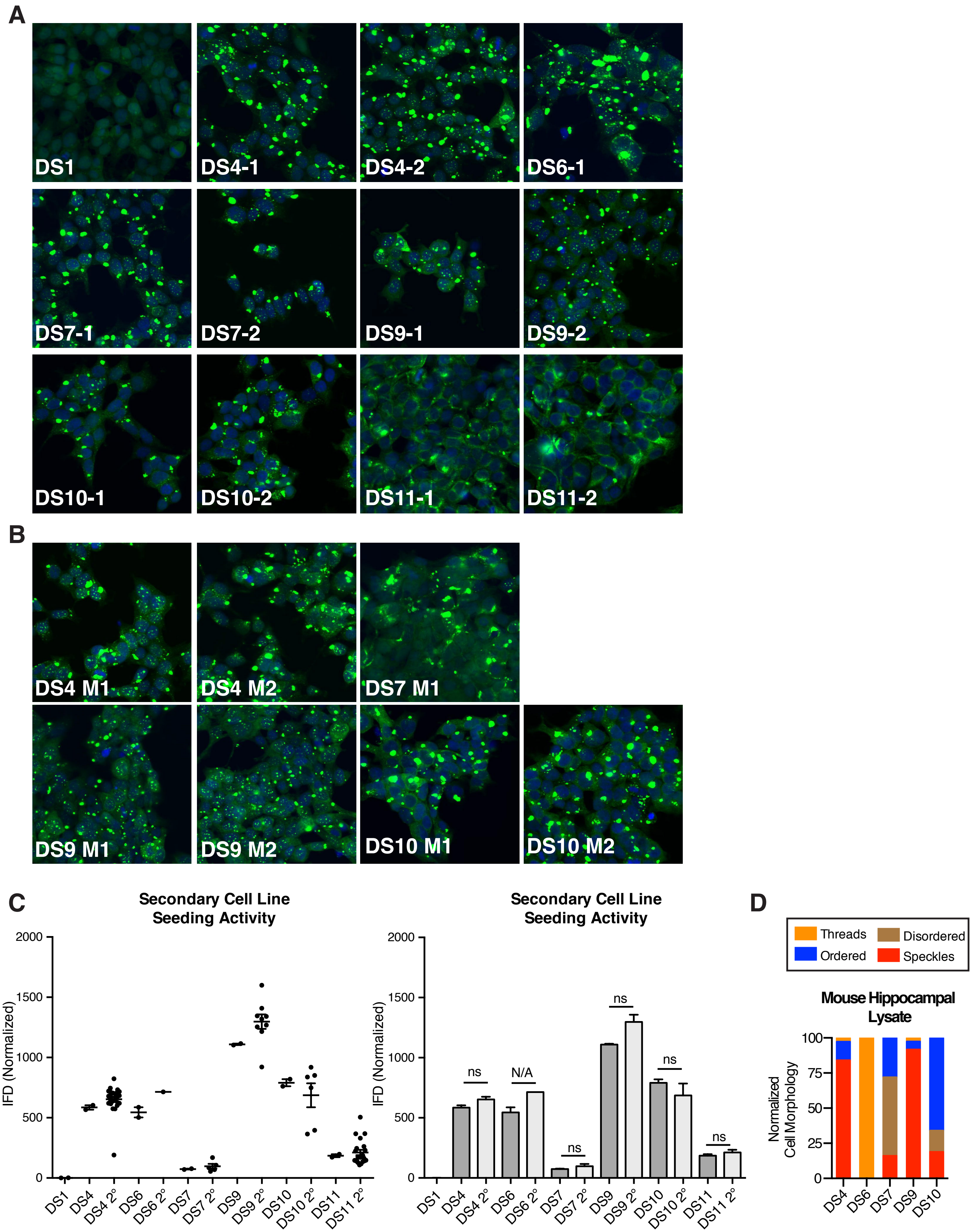
A
DS1
DS4-1
DS4-2
DS6-1
DS7-1
DS7-2
DS9-1
DS9-2
DS10-1
DS10-2
DS11-1
DS11-2
B
DS4 M1
DS4 M2
DS7 M1
DS9 M1
DS9 M2
DS10 M1
DS10 M2
C
Secondary Cell Line Seeding Activity
IFD (Normalized)
2000
1500
1000
500
0
DS1
DS4
DS4 2°
DS6
DS6 2°
DS7
DS7 2°
DS9
DS9 2°
DS10
DS10 2°
DS11
DS11 2°
Secondary Cell Line Seeding Activity
IFD (Normalized)
ns
N/A
ns
ns
ns
ns
D
Threads
Disordered
Ordered
Speckles
Mouse Hippocampal Lysate
Normalized Cell Morphology
100
75
50
25
0
DS4
DS6
DS7
DS9
DS10

Table S1, related to Figure 6. Summary of mice used in time course inoculation experiment
List of experimental mice discussed in this study, including sex, age at time of surgery, and age at time of tissue collection.

Table S2, related to Figure 3. Summary of mice used in strain panel inoculation experiment
List of experimental mice discussed in this study, including sex, age at time of surgery, and age at time of tissue collection.

Table S3, related to Figure 5. Summary of mice used in regional vulnerability inoculation experiment
List of experimental mice discussed in this study, including sex, age at time of surgery, and age at time of tissue collection.

Table S1. Summary of Mice Used in Time Course Inoculation Experiment

Time Course	N (Total)	Male	Female	Age at time of surgery (months)	Age at time of sacrifice (months)
4 weeks					
DS1	4	2	3	2-3	3-4
DS4	5	2	3	2-3	3-4
DS6	5	2	3	2-3	3-4
DS7	5	2	3	2-3	3-4
DS9	5	2	3	2-3	3-4
DS10	5	2	3	2-3	3-4
DS6 1:10	5	2	3	2-3	3-4
DS9 1:10	4	2	3	2-3	3-4
8 weeks					
DS1	4	2	2	2-3	3-4
DS4	5	3	2	2-3	3-4
DS6	5	3	2	2-3	3-4
DS7	5	3	2	2-3	3-4
DS9	5	3	2	2-3	3-4
DS10	5	3	2	2-3	3-4
DS6 1:10	4	2	2	2-3	3-4
DS9 1:10	4	2	2	2-3	3-4
12 weeks					
DS1	5	2	3	2-3	4-5
DS9	6	2	4	2-3	4-5
DS10	6	3	3	2-3	4-5
DS4	5	3	2	2-3	4-5
DS6	6	3	3	2-3	4-5
DS7	6	3	3	2-3	4-5
DS6 1:10	4	2	2	2-3	4-5
DS9 1:10	4	3	1	2-3	4-5

Table S2. Summary of Mice Used in Strain Panel Inoculation Experiment

Strain panel	N (Total)	Male	Female	Age at time of surgery (months)	Age at time of sacrifice (months)
DS1	6	2	4	2-3	4-5
DS2	3	1	2	2-3	4-5
DS3	3	1	2	2-3	4-5
DS4	3	1	2	2-3	4-5
DS5	3	1	2	2-3	4-5
DS6	3	2	1	2-3	4-5
DS7	3	1	2	2-3	4-5
DS8	3	1	2	2-3	4-5
DS9	3	2	1	2-3	4-5
DS10	3	2	1	2-3	4-5
DS11	3	1	2	2-3	4-5
DS12	3	1	2	2-3	4-5
DS13	3	1	2	2-3	4-5
DS14	3	1	2	2-3	4-5
DS15	3	1	2	2-3	4-5
DS16	3	1	2	2-3	4-5
DS17	3	1	2	2-3	4-5
DS18	3	1	2	2-3	4-5
DS19	3	1	2	2-3	4-5

Table S3. Summary of Mice Used in Regional Vulnerability Inoculation Experiment

Regional Vulnerability	N (Total)	Male	Female	Age at time of surgery (months)	Age at time of sacrifice (months)
DS1	3	2	1	3-3.5	4-5
DS4	3	1	2	3-3.5	4-5
DS6	3	1	2	3-3.5	4-5
DS7	3	1	2	3-3.5	4-5
DS9	3	1	2	3-3.5	4-5
DS10	3	1	2	3-3.5	4-5
DS11	3	1	2	3-3.5	4-5

Supplemental Experimental Methods

Tau purification and fibrillization

Recombinant full-length (FL) 2N4R tau protein was prepared as previously described (Goedert and Jakes, 1990). pRK172 FL 2N4R tau was expressed in Rosetta (DE3)pLACI competent cells (Novagen) and tau was purified according to established protocols. After purification, tau was lyophilized using a FreeZone Plus Freeze Dry System (Labconco) and stored at -80°C as single-use aliquots. Prior to fibrillization, monomeric tau was re-suspended in 25 mM DTT for 45 minutes. The protein was then fibrillized at a final concentration of 8 μM in tau buffer (2.5 mM DTT/10 mM HEPES pH=7.4/100 mM NaCl/8 μM heparin, final volume of 200μL) at 37°C for 24 hours prior to addition to cells.

Cell culture

All HEK293T and HEK293 cell lines were grown in complete media: Dulbecco's Modified Eagle's Medium (DMEM) (Gibco) with 10% fetal bovine serum (HyClone) and 1% penicillin/streptomycin (Gibco). Cells were cultured and passaged at 37°C, 5% CO_2, in a humidified incubator. Dulbecco's phosphate buffered saline (Life Technologies) was used for washing the cells prior to trypsinization with 0.05% Trypsin-EDTA (Life Technologies).

Lentivirus production

Lentivirus was prepared as previously described (Araki et al., 2004; Sanders et al., 2014). HEK293T cells were plated at $1x10^6$ cells/well in 6-well plates. After 24 hours, cells were transfected with a three-component plasmid system for virus production: VSV-G (400 ng), PSP (1200 ng), FM5 (400 ng). DNA was mixed with 7.5μL TransIT-293 (Mirus) and 250μL OptiMEM for 15 minutes prior to addition to cell media. After 48 hours, media was harvested and spun at 500 x g for 5 minutes to remove debris. For generation of HEK293 cell lines, lentivirus-containing supernatant was stored at -80°C prior to addition to cells. For primary neurons, lentiviral supernatant was concentrated 50x using lenti-X concentrator (Clontech) according to manufacturer's protocol. The final concentrated virus was re-suspended in PBS with 25 mM HEPES (pH = 7.4).

Stable HEK293 cell line generation

Monoclonal HEK293 cell lines were generated that stably overexpress fusion proteins containing the tau repeat domain (amino acids 244-372 of the 2N4R isoform of tau) with various mutations (P301L, P301S, V337M) previously shown to cause familial tauopathy (FTDP-17) (Hutton et al., 1998). Two monoclonal HEK293 cell lines were previously described: Clone 1/DS1, which expresses tau RD(P301L/V337M)-YFP (Sanders et al., 2014) and the tau RD(P301S) FRET biosensor (ATCC CRL-3275), which expresses tau RD(P301S)-CFP and tau RD(P301S)-YFP (Holmes et al., 2014). To generate additional polyclonal lines, HEK293 cells were plated at 50,000 cells/well in a 12-well plate. After 18 hours, 300μL conditioned media containing lentivirus was added to the wells (RD LM FRET polyclonal: 150 μL tau RD(P301L/V337M)-CFP and 150 μL tau RD(P301L/V337M)-YFP; RD P301S split-luciferase polyclonal: 150μL tau RD(P301S)-Cluc and 150μL tau RD(P301S)-Nluc). For both polyclonal lines, cells were given 3 days to grow in the presence of virus. Cells were then re-plated in a 10 cm dish, grown to confluency, and stored in liquid nitrogen until use.

To generate monoclonal lines, the two polyclonal populations (RD LM FRET and RD P301S split-luciferase) were diluted sparsely in 10 cm dishes, so that there were fewer than 30 cells per dish. Cells were given seven days to grow into visible colonies. At this point, cloning cylinders (Bel-Art Products) were used to isolate single colonies, which were passaged to new wells. Monoclonal lines were serially amplified to confluency using 24-well then 6-well then 10 cm dishes. Upon reaching confluency in 10 cm dishes, monoclonal lines were frozen in liquid nitrogen until use. LM10 was the tenth monoclonal line selected from the RD LM FRET polyclonal, and was chosen due to its ability to differentiate toxic and non-toxic strains (described below). The RD P301S-split luciferase biosensor was selected due to its high signal to noise ratio in differentiating lysates with and without aggregates.

Lysate production for generation of strain library

Confluent cells from 6-well plates were harvested, pelleted, and stored at -80°C for the following cell lines (Sanders et al., 2014): Clone 1-derived (Clone 1, Clone 9, Clone 10), OFF1-derived (AGD2/mosaic, CBD3/disordered, CBD5/disordered, CBD3/speckles, AD1/speckles, PiD2/ordered). Cell pellets were thawed on ice and subsequently lysed in PBS with 0.05% Triton X-100 and a cOmplete mini protease inhibitor tablet (Roche) by triturating 10x and incubating at 4°C for 10 minutes. Sequential 5-minute centrifugations were then performed at 500 x g and 1000 x g to clarify the lysate. A Bradford assay (Bio-Rad) was performed on the supernatants, and protein concentrations were normalized to 5 μg/μL with addition of lysis buffer. Lysates were stored at -80°C prior to addition to cells.

To produce brain homogenates, the following samples were used: transgenic P301S mouse brain (age = 9 months), an Alzheimer's disease patient brain (patient AD1) (Sanders et al., 2014), and a late-stage chronic traumatic encephalopathy patient brain that was a generous gift from Dr. Ann McKee. For each, 0.4 gram sections were sonicated in 5 mL TBS with cOmplete protease inhibitors (Roche) using an Omni-Ruptor 250 probe sonicator at 30% power for 3-second pulses x 30 cycles. Crude homogenates were then clarified by centrifugation at 15,000 x g for 15 minutes. The supernatants were set aside, a Bradford was performed, and protein concentrations were normalized to 4 μg/μL with addition of TBS buffer. Homogenates were stored at -80°C prior to addition to cells.

Generation of a library of monoclonal strains

To generate a library of isogenic tau strains, several monoclonal tau RD(P301L/V337M)-YFP cell lines were examined for their ability to stably propagate a diversity of strains. Clone 1/DS1 (Sanders et al., 2014) was selected for its capacity to amplify both highly toxic strains and strains prone to sectoring, which can be attributed to its intermediate level of tau RD expression. Clone 1 cells were plated at 240,000 cells/well in 12-well plates. After 24 hours, cells were treated with 400 nM tau fibrils or 20 μg lysate/homogenate (see lysate production for generation of strain library), and prepared as transduction complexes (4μL lipofectamine-2000 (Life Technologies), protein source, and OptiMEM to 200μL volume). After 18 hours, cells were washed, trypsinized, and re-plated in a 6-well plate. At confluency (day 3), cells were diluted sparsely in 3 x 10 cm dishes (per condition) so that there were less than 30 cells per dish. Cells were given 9 days to amplify into visible colonies. At day 12, epifluorescence microscopy was used to find colonies featuring cells with inclusions and these were marked. Cloning cylinders (Bel-Art Products) were used to isolate up to six colonies per condition, and each individual colony was separately amplified to confluency in 12-well, then 6-well, and 10 cm dishes. At approximately day 30, cells were either plated on coverslips for fixation and confocal microscopy or were frozen down in single-use pellets at -80°C for analysis by seeding and protease digestion. A total of 90 monoclonal lines were examined. Based on preliminary analysis by inclusion morphology, seeding, and protease digestion, 21 were selected for rigorous analysis by both the aforementioned assays as well as sedimentation analysis and toxicity assays. Finally, 18 lines were suspected to be distinct strains and were designated DS2 to DS19 (DS = David/Sarah).

Fixation of cells for confocal microscopy

Cells were grown for 48 hours on coverslips in 24-well plates. Media was removed and replaced with 4% PFA for 15 minutes. PFA was removed and replaced with PBS. Cells were washed once with additional PBS and DAPI-stained for 10 minutes in 0.1% Triton-X. Stain was removed and replaced with PBS. Coverslips were mounted using Prolong Gold Antifade reagent (Life Technologies), sealed with nail polish, and placed at 4°C prior to confocal analysis.

Confocal analysis of strains based on inclusion morphology

For confocal microscopy, a Zeiss Axiovert 200M microscope was coupled to a Zeiss LSM 5 PASCAL system. For the collection of all images, a pinhole size of 0.8 μm was used. Representative images of each monoclonal cell line were taken and were scored based on inclusion morphology: diffuse (no aggregates), mosaic (loss of aggregated state with division), ordered (large, dense juxtanuclear inclusion with no nuclear aggregates), speckles (small juxtanuclear inclusion with numerous nuclear speckles), threads (long, fibril-like inclusions in cytoplasm with rare nuclear speckles), disordered (diffuse aggregates that wrapped around nucleus with no nuclear speckles).

For blinded analysis of strain phenotype, images were collected with the In Cell Analyzer 6000 at 40x resolution with the assistance of the UTSW HTS Core facility. Images were coded and a blinded counter scored aggregate morphology according to the previously established guidelines discussed above (Sanders et al., 2014). Decoding was performed after completion of blinded counting, and morphology counts were normalized to total number of aggregate-positive cells.

Limited proteolysis

Lyophilized pronase (Roche) was re-suspended in PBS to a final concentration of 1 mg/mL and aliquots were snap-frozen and placed at -80°C. Cell pellets were thawed on ice and lysed in PBS with 0.05% Triton X-100 and a cOmplete mini protease inhibitor tablet (Roche) by triturating 10x and incubating at 4°C for 10 minutes. Sequential 5 minute centrifugations were then performed at 500 x g and 1000 x g to clarify the lysate. A Bradford assay (Bio-Rad) with BSA standard curve was performed and protein concentrations were normalized to 4 µg/µL with addition of lysis buffer. 60 µg (15 µL) of cell lysate was added to 15 µL of pronase (diluted in PBS) at a concentration of 60 µg/mL for a final volume of 30 µL and a final pronase concentration of 30 µg/mL. Cell lysates were digested at 37°C for one hour. Reactions were quenched by addition of 30 µL 2x sample buffer (4 µL BME, 11 µL 10% SDS, 15 µL 4x Laemmli buffer) followed by five minutes of boiling. 13 µL of each sample was loaded onto a NuPAGE 10% Bis-Tris gel (Life Technologies). Gels were run at 150 V for 70 minutes. Protein was transferred to Immobilon P (Millipore) using a semi-dry transfer apparatus (Bio-Rad). Membranes were blocked for 1 hour in 4% milk. Membranes were probed for tau using mouse monoclonal anti-tau 2B11 (0.7 µg/µL, Clontech) for 18 hours, washed four times with TBS-T, counter-probed with goat anti-mouse HRP (1:4000, GE Healthcare) for 1.5 hours, and were washed four additional times with TBS-T. Finally, membranes were exposed to ECL Prime Western Blotting Detection System (Fisher Scientific) for 2 minutes and were developed using a digital Syngene imager. For diluted strain limited proteolysis, 40 µg of strain cell lysate, or 20 µg of strain lysate mixed with 20 µg of HEK lysate were digested at 37°C for 90 minutes. In place of the relatively expensive 2B11 antibody, blots were developed using an antibody produced in bulk against amino acids 244-266 of wild type human 4R tau protein. This rabbit antibody was used at a working concentration of 1.35 µg/mL, and blots were otherwise developed as above.

Sedimentation analysis and densitometry of strain library

Cell lysates were prepared and clarified as described above (see Limited proteolysis) in biological quadruplicates for each strain. A Bradford assay (Bio-Rad) with BSA standard curve was performed to determine the protein concentrations for the 76 samples, normalizing each to 1.6 µg/µL. 1 mL of each was centrifuged at 186,000 x g for 60 minutes, with the remainder being set aside as the total fraction. After centrifugation, the supernatant fraction was placed aside and the pellet was washed with 1 mL lysis buffer. The ultracentrifugation step was repeated for 30 minutes, and the wash fraction was aspirated. Final pellets were re-suspended in 1 mL of 4% SDS/1% BME (in PBS) with the aid of five minutes of boiling. For each sample, 1 µg total (or equivalent volume of supernatant or pellet) was run on a NuPAGE 10% Bis-Tris gel (Life Technologies) at 150 V for 35 minutes. Protein was transferred to Immobilon P (Millipore) using a semi-dry transfer apparatus (Bio-Rad). Membranes were blocked for 1 hour in 4% milk and then probed overnight with rabbit polyclonal anti-tau ab64193 (1:5000, AbCam) and rabbit polyclonal anti-cofilin (1:28,000, Sigma). Following four washes with TBS-T, blots were counter-probed with goat anti-rabbit HRP (1:4000, Jackson Immunotherapy) for 90 minutes at room temperature. Finally, blots were washed an additional four times and membranes were imaged with a digital Syngene imager following exposure to ECL Prime Western Blotting Detection System (Fisher Scientific) solution for two minutes. Biological replicates were imaged separately, with four blots being developed at a time. Densitometric units were calculated using Syngene GeneTools software with manual band quantification. The brightness of each tau band (total, supernatant, pellet) was normalized relative to the signal calculated for the condition’s associated total cofilin. Ratios were then averaged across biological quadruplicates.

Split-luciferase complementation assay

A monoclonal HEK293 cell line expressing tau RD (P301S)-Cluc and tau RD (P301S)-Nluc was generated (see Stable HEK293 cell line generation) and plated at 24,000 cells/well in 96-well plates. After 18 hours, when the cells were at 50% confluency, cells were transduced with cell lysate: indicated amounts of clarified cell lysate (see Limited Proteolysis) were added in transfection complexes with 0.4 µL lipofectamine-2000 (Life Technologies) to each well. 60 hours after addition of lysate, media was aspirated and replaced with luciferin solution (150 µg/mL D-luciferin potassium salt, Gold Biosciences, in Dulbecco's phosphate-buffer saline, Gibco). Cells were incubated in luciferin solution for two minutes at 37°C prior to reading luminescence with a Tecan M1000 fluorescence plate reader. Each condition was performed in biological quadruplicate with each replicate being performed on a separate plate to control for differences between plates. The seeding ratio was calculated relative to sham control for an individual plate. Seeding ratios were then averaged across quadruplicates and standard errors of the mean were calculated and plotted. Inflection point was defined as the amount of lysate required to achieve a 50% increase in luminescence relative to sham treatment. EC_{50} and peak seeding were calculated using a non-linear regression with one-phase decay fit.

Toxicity assay

A monoclonal cell line expressing tau RD (P301L/V337M)-CFP and tau RD (P301L/V337M)-YFP was generated and given the name LM10 (see Stable HEK293 cell line generation). LM10 cells were plated at 240,000 cells/well of 12-well plates. After 18 hours, wells were transduced with 20 µg clarified lysate (see Limited Proteolysis) in transfection complexes with 4 µL lipofectamine-2000. Each condition was performed in biological triplicate. After 24 hours, media was aspirated and cells were trypsinized and re-plated into 6-well plates. After 48 hours (i.e. 72 hours post-treatment), media was removed, cells were trypsinized, and pelleted, followed by resuspension in flow cytometry buffer (HBSS with 1% FBS and 1 mM EDTA). FRET-positive (aggregate-containing) and FRET-negative (aggregate-lacking) cells were gated according to published protocols (Furman et al., 2015; Holmes et al., 2014). Using a FACS Aria II SORP cell sorter (BD Biosciences), 7000 FRET-positive cells were collected in 1.4 mL media for each condition (DS2 to DS19). For the negative control (DS1), 7000 FRET-negative cells were sorted. 200 µL (i.e. 1000 cells) were plated in sextuplicate for each condition in 96-well plates. Cells were given 7 days to amplify. Cells were then harvested with 0.05% trypsin, pelleted, and fixed in 2% paraformaldehyde (Electron Microscopy Services) for 10 minutes. Cells were re-pelleted and resuspended in flow cytometry buffer. A MACSQuant VYB (Miltenyi) was used to perform FRET flow cytometry according to previously published protocols (Holmes et al., 2014), and total FRET-positive and FRET-negative cells were counted for each condition. Totals were averaged across technical sextuplicates and then averaged across biological triplicates. Error bars represent the standard error of the mean for biological triplicates.

Statistical analysis of *in vitro* correlations

For the correlation of toxicity, seeding, and sedimentation metrics, normality of the data was assessed using both D'Agostino/Pearson and Shapiro-Wilk tests. If both tests were passed, data sets were considered normal and a Pearson correlation was performed. Else, the data sets were not considered normal and a more conservative Spearman correlation was performed. Correlations were considered significant if p was less than or equal to 0.05.

Primary neuron culture and staining

Cortical and hippocampal neurons were isolated from E18.5 CD1 mice and cultured according to previous literature (Yano et al., 2014). Briefly, neurons were incubated with 0.5% trypsin in HBSS with glucose (1:6 dilution) for 20 minutes at 37°C. Subsequently, neurons were triturated and passaged through a 70 µm filter, followed by plating 100,000 cells per well on poly-D lysine- or polyethyleneimine (PEI)-coated plates for cortical or hippocampal cultures respectively. Neurons were treated at DIV3 with 2 µL of 50x-concentrated 1N4R tau(P301S)-YFP lentivirus (see Lentivirus production) per well of a 96-well plate. Neurons were subsequently treated at DIV6 with 10 µg of cell lysate or PBS. Neurons were examined for intracellular aggregates each day with an epifluorescence microscope (Nikon Eclipse TI), and scored using a 0-5 scale (No seeding – Peak seeding). Neurons were fixed at 5, 8 or 11 days post lysate addition with a modified triton-X extraction to remove soluble tau protein (Volpicelli-Daley et al., 2011). Briefly, cells were incubated with 4% PFA/4% sucrose in PBS with 1% Triton-X 100 for 30 minutes. Cells were subsequently washed and stained with MC1 antibody (1:500; Peter Davies) in 10% NGS in PBS overnight at 4°C. Cells were washed and treated with anti-mouse IgG 546 (1:400, Life Technologies), and stained with DAPI. Cells were imaged with the In Cell Analyzer 6000 at 40x resolution with the assistance of the University of Texas Southwestern Medical Center HTS Core facility.

Monoclonal Secondary Cell Line Isolation and Characterization

Cell lysate or mouse brain homogenate was transduced into the LM1 cell line. After four days in culture, single cells were sorted into 5 x 96 wells per condition. Cells were allowed to grow for 7-10 days prior to amplification into 24-well dishes, and subsequently expanded into larger dishes. Cell pellets were collected for seeding assay experiments. Monoclonal cell lines were plated on 96-well plates, fixed with 4% paraformaldehyde, and stained with DAPI. These lines were subsequently imaged with the In Cell Analyzer 6000 at 40x resolution with the assistance of the UTSW HTS Core facility.

Primary neuron seeding assay

Hippocampal neurons were plated at 75,000 cells per well on PEI-coated plates. At DIV3, cells were treated with 1µL of 50x concentrated tau RD(P301S)-CFP and 1µL of tau RD(P301S)-YFP lentivirus. AT DIV6, cells were treated with 10µg of cell lysate or an equivalent volume of PBS. Cells were subsequently incubated for four days. A MACSQuant VYB (Miltenyi) flow cytometer was used to assess FRET-positive neurons according to previously published literature (Furman et al., 2015; Holmes et al., 2014).

Cell lysate production for animal inoculation experiments

DS1-19 cell lines were grown in 3 x 10cm dishes until 90% confluency. Cells were trypsinized, re-suspended in media and centrifuged at 500 x g. Cell pellets were washed with 1x PBS and stored at -80°C until use. Pellets were thawed on ice and re-suspended in 1x PBS with cOmplete protease inhibitors (Roche) using an Omni-Ruptor 250 probe sonicator at 30% power for 30, 3 second cycles. The probe sonicator was washed with 100% ethanol and ddH_2O between cell lines. Strains were subsequently centrifuged at 1000 x g, normalized to 7µg/µl by Bradford assay (Bio-Rad) and stored as aliquots at -80°C until use.

Sedimentation analysis and densitometry of injected lysates

Sonicated and clarified cell lysate was thawed on ice, and diluted to 2 µg/µL in 1x PBS with cOmplete protease inhibitors (Roche). Samples were subdivided into a total protein and ultracentrifuge (UC) aliquots. The UC aliquots were centrifuged at 186,000 x g for 90 minutes. Supernatant was removed and stored with the total lysate aliquot at -80°C until use. Pellets were washed with 1x PBS and centrifuged at 186,000 x g for an additional 30 minutes. Pellets were re-suspended to their original volume. SDS-PAGE was performed on total, soluble or insoluble fractions of each cell line (1:2:1 ratio) using 5-20% gradient acrylamide gels. Gels were transferred as described above. Membranes were cut at the 20kDalton ladder mark and incubated at 4°C overnight with a rabbit polyclonal anti-tau antibody (1:4000, Abcam ab64193) or a rabbit polyclonal anti-cofilin antibody (1:4000; Sigma). Anti-rabbit ECL HRP conjugated secondary antibody (1:4000, GE Lifesciences) was added for one hour, and blots were developed using ECL Prime Western Blotting Detection System (Fisher Scientific). Washes were performed as described above. Densitometry was performed by measuring the mean grey value (mgv) of bands with ImageJ, and normalizing to cofilin mgv. Samples were averaged across biological triplicate. A one-way ANOVA with Bonferroni's multiple comparisons correction was performed by comparing DS1-1 to each sample. A one-way t-test was performed to directly compare DS10 and DS4.

Animal maintenance

We obtained transgenic mice that express 4R1N P301S human tau under the murine prion promoter {Yoshiyama:2007bf} from Jackson Laboratory, and maintained them on a B6C3 background. Transgenic mice and wild-type littermates were housed under a 12 hour light/dark cycle, and were provided food and water *ad libitum*. All experiments involving animals were approved by the University of Texas Southwestern Medical Center institutional animal care and use committee.

Inoculation experiments

P301S mice were anesthetized with isoflurane and kept at 37°C throughout the inoculation. Mice were injected with separate 10 μL gas-tight Hamilton syringes for each strain at a rate of 0.2 μL per minute. For strain panel and time course experiments (Figures 3.5, 3.11, 3.13), animals were inoculated with 10 μg (1.428 μL) of cell lysate in the left hippocampus (from bregma: -2.5 mm posterior, -2 mm lateral, -1.8 mm ventral). For the regional vulnerability experiments (Figure 3.9), animals were injected at six sites (x, y, z from bregma: sensory cortex: -2.75, -0.2, -0.5; caudate/putamen: -2.75, -0.2, -2.8; visual cortex: -1.9, -2.9, -0.45; hippocampus: -1.9, -2.9, -1.4; thalamus: -1.9, -2.9, -4; inferior colliculus: -1, -5.6, -1.5) with 5 μg of lysate per region.

Animal tissue collection

P301S or WT mice were anesthetized with isoflurane and perfused with chilled PBS + 0.03% heparin. Brains were post-fixed in 4% paraformaldehyde overnight at 4°C and then placed in 30% sucrose in PBS until further use.

Histology

Brains were sectioned at 50μm using a freezing microtome. Slices were first blocked for one hour with 5% milk in TBS with 0.25% Triton X-100 (blocking buffer). For DAB stains, brain slices were incubated with biotinylated AT8 antibody (1:500, Thermo Scientific) overnight in blocking buffer at 4°C. Slices were subsequently incubated with the VECTASTAIN Elite ABC Kit (Vector Labs) in TBS prepared according to the manufacturer's protocol for 30 minutes, followed by DAB development using the DAB Peroxidase Substrate Kit with the optional nickel addition (Vector Labs). Slices were imaged using the Olympus Nanozoomer 2.0-HT (Hamamatsu). For astrocyte staining, slices were permeablized in 0.25% Triton X-100 in TBS, followed by blocking with 3% milk and 10% normal goat serum (NGS) for 30 minutes, followed by incubation with AT8 (1:500, Thermo Scientific) and GFAP (1:500, Dako) overnight at 4°C. For microglial staining, slices were treated with AT8 as above, and Iba1 (1:500, Dako). Slices were incubated with 1:500 anti-mouse 488 and anti-rabbit 546 antibodies for astrocyte staining (Life Technologies). Slices were imaged followed by imaging using a Zeiss LSM780 inverted confocal microscope. For microglial staining, slices were incubated in 1:500 anti-mouse 546 and anti-rabbit 488. Slices were imaged using a Zeiss Axioscan.Z1 at 40x resolution, or with a Zeiss LSM780 inverted confocal microscope.

Quantification of Tau pathology

Images of AT8 DAB stained slices were collected as above. A blinded analysis of the level of tau pathology was performed using a semi-quantitative 0-3 scale (no pathology, mild, moderate, and severe, respectively) as previously reported (Lace et al., 2009). Briefly, images of each brain slice were randomized and blinded to the scorer. Individual brain regions in each slice were assessed for AT8 positive neuronal inclusions. Scores were recorded unless a slice was damaged such that the region of interest was not present in the slice. The level of pathology was averaged among biological replicates for each region within a condition. For the regional vulnerability experiments (Figure 5), pathology was normalized by subtracting the average DS1 pathology in a region, and heat maps were generated with discrete bins for different pathology levels as described within the figure. For the time course experiments (Figure 7), averages were plotted as a heat map with a gradient from 0 to 3 as reported in the figure. Heat maps were generated using MATLAB.

Quantification of Iba1 microglial pathology

Slices from mice 12 weeks after inoculation with DS1, 4, 6, 7, 9, or 10 were stained for Iba1 as above. Hippocampi at the level of the injection site were outlined as a region of interest, and microglia were quantified in a blinded fashion for cellular morphology within this region of interest. Microglia were scored as ramified, rod, or activated non-rod morphologies. Microglial counts were averaged within a condition, and normalized to total area assessed.

P301S FRET Flow Seeding assay

Bilateral hippocampus, sensory cortex, or thalamic 1mm punches were isolated from mice injected with DS1, 4, 6, 7, 9, 10 or diluted DS6 and DS9, 8-weeks post inoculation. Samples were placed into 1xTBS at a dilution of $1mm^3/mL$ (v/v) and sonicated with a water bath sonicator (Qsonica Q700MPX with chiller and tubing set) at 4°C at 50% power for 30 minutes. Seeding assays were performed as previously described (Furman et al., 2015; Holmes et al., 2014). Briefly, 2.5 µL of each sample was added in triplicate to wells of a 96-well plate onto the tau RD(P301S) FRET biosensor cell line. Cells were incubated for 48 hours and then trypsinized, fixed with 2% PFA in 1x PBS, and incubated in flow cytometry buffer. A FACS LSRFortessa SORP was used to perform FRET flow cytometry as previously described (Furman et al., 2015; Holmes et al., 2014). Integrated FRET density (IFD = percent cells positive for FRET multiplied by the median fluorescent intensity of FRET-positive cells) was averaged for every condition and normalized to lipofectamine-2000 (sham) IFD. A one-way ANOVA with Bonferroni corrections was performed for each region by comparing DS1 ipsilateral IFD to all other conditions within that region. For seeding of secondary monoclonal lines, the original monoclonal cell lines and secondary cell lines were prepared in PBS with 0.05% Triton X-100 with cOmplete mini protease inhibitors as described above. FRET biosensor cells were incubated with 2 µg of lysate per well, and cells were harvested at 24 hours post-transduction. Two separate cell pellets were prepared to assess the seeding activity of the original strains. A two-tailed student t-test was performed to compare seeding activity between the original cell line samples and secondary cell lines (ns for $P \geq 0.05$).

Supplemental References

Araki, T., Sasaki, Y., Milbrandt, J., 2004. Increased nuclear NAD biosynthesis and SIRT1 activation prevent axonal degeneration. Science 305, 1010–1013. doi:10.1126/science.1098014

Furman, J.L., Holmes, B.B., Diamond, M.I., 2015. Sensitive Detection of Proteopathic Seeding Activity with FRET Flow Cytometry. J Vis Exp e53205–e53205. doi:10.3791/53205

Goedert, M., Jakes, R., 1990. Expression of separate isoforms of human tau protein: correlation with the tau pattern in brain and effects on tubulin polymerization. EMBO J. 9, 4225–4230.

Holmes, B.B., Furman, J.L., Mahan, T.E., Yamasaki, T.R., Mirbaha, H., Eades, W.C., Belaygorod, L., Cairns, N.J., Holtzman, D.M., Diamond, M.I., 2014. Proteopathic tau seeding predicts tauopathy in vivo. Proceedings of the National Academy of Sciences 111, E4376–E4385. doi:10.1073/pnas.1411649111

Hutton, M., Lendon, C.L., Rizzu, P., Baker, M., Froelich, S., Houlden, H., Pickering-Brown, S., Chakraverty, S., Isaacs, A., Grover, A., Hackett, J., Adamson, J., Lincoln, S., Dickson, D., Davies, P., Petersen, R.C., Stevens, M., de Graaff, E., Wauters, E., van Baren, J., Hillebrand, M., Joosse, M., Kwon, J.M., Nowotny, P., Che, L.K., Norton, J., Morris, J.C., Reed, L.A., Trojanowski, J., Basun, H., Lannfelt, L., Neystat, M., Fahn, S., Dark, F., Tannenberg, T., Dodd, P.R., Hayward, N., Kwok, J.B., Schofield, P.R., Andreadis, A., Snowden, J., Craufurd, D., Neary, D., Owen, F., Oostra, B.A., Hardy, J., Goate, A., van Swieten, J., Mann, D., Lynch, T., Heutink, P., 1998. Association of missense and 5'-splice-site mutations in tau with the inherited dementia FTDP-17. Nature 393, 702–705. doi:10.1038/31508

Lace, G., Savva, G.M., Forster, G., de Silva, R., Brayne, C., Matthews, F.E., Barclay, J.J., Dakin, L., Ince, P.G., Wharton, S.B., MRC-CFAS, 2009. Hippocampal tau pathology is related to neuroanatomical connections: an ageing population-based study. Brain 132, 1324–1334. doi:10.1093/brain/awp059

Sanders, D.W., Kaufman, S.K., DeVos, S.L., Sharma, A.M., Mirbaha, H., Li, A., Barker, S.J., Foley, A.C., Thorpe, J.R., Serpell, L.C., Miller, T.M., Grinberg, L.T., Seeley, W.W., Diamond, M.I., 2014. Distinct Tau Prion Strains Propagate in Cells and Mice and Define Different Tauopathies. Neuron 1–18. doi:10.1016/j.neuron.2014.04.047

Volpicelli-Daley, L.A., Luk, K.C., Patel, T.P., Tanik, S.A., Riddle, D.M., Stieber, A., Meaney, D.F., Trojanowski, J.Q., Lee, V.M.-Y., 2011. Exogenous α-Synuclein Fibrils Induce Lewy Body Pathology Leading to Synaptic Dysfunction and Neuron Death. Neuron 72, 57–71. doi:10.1016/j.neuron.2011.08.033

Yano, H., Baranov, S.V., Baranova, O.V., Kim, J., Pan, Y., Yablonska, S., Carlisle, D.L., Ferrante, R.J., Kim, A.H., Friedlander, R.M., 2014. Inhibition of mitochondrial protein import by mutant huntingtin. Nat Neurosci 17, 822–831. doi:10.1038/nn.3721